Recent Progress in Polymer Solar Cells: Manipulation of Polymer:Fullerene Morphology and the Formation of Efficient Inverted Polymer Solar Cells

By *Li-Min Chen, Ziruo Hong, Gang Li,* and *Yang Yang**

Polymer morphology has proven to be extremely important in determining the optoelectronic properties in polymer-based devices. The understanding and manipulation of polymer morphology has been the focus of electronic and optoelectronic polymer-device research. In this article, recent advances in the understanding and controlling of polymer morphology are reviewed with respect to the solvent selection and various annealing processes. We also review the mixed-solvent effects on the dynamics of film evolution in selected polymer-blend systems, which facilitate the formation of optimal percolation paths and therefore provide a simple approach to improve photovoltaic performance. Recently, the occurrence of vertical phase separation has been found in some polymer:fullerene bulk heterojunctions.[1–3] The origin and applications of this inhomogeneous distribution of the polymer donor and fullerene acceptor are addressed. The current status and device physics of the inverted structure solar cells is also reviewed, including the advantage of utilizing the spontaneous vertical phase separation, which provides a promising alternative to the conventional structure for obtaining higher device performance.

1. Introduction

The discovery of semiconducting (conjugated) polymers stimulated the research field of organic electronics.[4,5] The development of a variety of organic-based optoelectronics, such as diodes,[6] light-emitting diodes,[7–9] photodiodes/solar cells,[10–13] field-effect transistors,[14–17] and memory devices[18–21] have been reported, providing appealing alternatives to inorganic-based electronics.

The large exciton-binding energy in a polymeric matrix results in strongly localized electron–hole pairs upon light absorption, giving rise to the small exciton-diffusion length and inefficient exciton dissociation. Therefore, a major challenge lies in fabricating polymer solar cells, in which free-charge-carrier generation is a critical step. Fortunately, it has been found that efficient charge transfer can take place between materials, that is, donor and acceptor molecules, with suitable energy-level offsets. The strong electric field at the molecular interface of two materials with different electrochemical potentials is capable of separating the excitons into weakly-bounded Coulombic pairs, and thereafter separated charge carriers. In cases where the donor and acceptor molecules form an intimate contact in blend films, efficient charge transfer takes place with an efficiency approaching 100%. The short exciton diffusion length (5–10 nm), which is much smaller than the necessary film thickness for effective optical absorption, has limited the external quantum efficiency (EQE) and hampered efficient utilization of the photogenerated excitons in organic photovoltaics. A major breakthrough was achieved with the bulk heterojunction (BHJ) concept, where the nanoscale phase separation creates donor/acceptor interfaces for exciton dissociation via efficient charge transfer from donor to acceptor throughout the film.[12] The concepts of donor/acceptor and BHJs, thus, establish the cornerstones of polymer solar cells.

Despite the high attainable EQE, overall power conversion efficiencies (PCE) reported are still low, due to the inferior charge-transport properties and limited spectral absorption range of the polymer active layer. On one hand, endeavors in synthesis and development of novel low-band-gap polymers are being carried out to harvest the major part of the solar spectrum.[22–28] On the other hand, film-growth dynamics of polymer blends via solution processes has become one of the central topics to derive maximal efficiency from bulk-heterojunction structures. Meanwhile, precise efficiency measurements provide solutions to the spectral mismatch between the solar spectrum and polymer absorption, offering accurate evaluation of novel photoactive materials.[29,30]

High internal quantum efficiencies can be expected, provided that efficient donor-to-acceptor charge transfer and transport in the bulk heterojunctions occurs. A suitable energy-level alignment between the donor and acceptor to provide the driving force for charge transfer as well as a large ratio of interfacial area to

---

[*] Prof. Y. Yang, L.-M. Chen, Z. Hong
Department of Materials Science and Engineering
University of California, Los Angeles
Los Angeles, CA 90095 (USA)
E-mail: yangy@ucla.edu

Dr. G. Li
Solarmer Energy, Inc.
3445 Fletcher Ave
El Monte, CA 91731 (USA)

DOI: 10.1002/adma.200802854

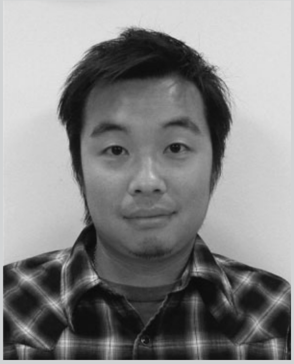

Li-Min (Raymond) Chen has been a Ph.D. student in Prof. Yang Yang's group in the Department of Materials Science and Engineering at University of California, Los Angeles since 2006. He obtained his B.S. and M.S. at National Cheng Kung University (Taiwan) in 2002 and 2004, respectively. His research focuses on inverted structure polymer solar cells and transparent conductor applications.

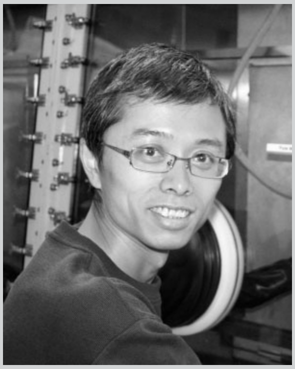

Zirou Hong has been a postdoctoral researcher in Prof. Yang Yang's group in the Department of Materials Science and Engineering at UCLA since 2007. He obtained his Ph.D. in Condensed Matter Physics (advisor: Prof. Wenlian Li) at Chinese Academy of Sciences in 2001. He has also conducted research at COSDAF, City University of Hong Kong and Institut für Angewandte Photophysik (IAPP), TU Dresden. His research is focused on organic/polymeric opto-electronics, especially electroluminescence and photovoltaics.

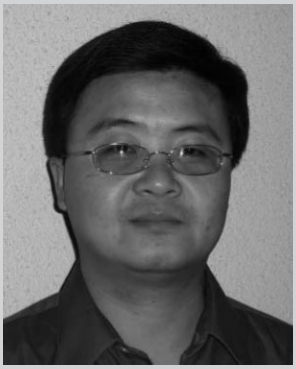

Gang Li is a Technology Researcher at Solarmer Energy, Inc., in El Monte, CA. He has been a postdoctoral researcher in Prof. Yang Yang's group in the Department of Materials Science and Engineering at UCLA from 2004 to 2007. He obtained a B.S. at Wuhan University (China) in 1994, and a Ph.D. in Condensed Matter Physics at Iowa State University in 2003, focusing on organic light-emitting devices (OLEDs). His current research focus is polymer solar cells.

volume for efficient charge dissociation are prerequisites to ensure that charge transfer is the dominant decay channel of photogenerated excitons. As a consequence, a bicontinuous percolation pathway must be formed for the photogenerated holes and electrons to reach their respective contacts for efficient charge collection. Therefore, the nanoscale phase-separation morphology plays a decisive role linking the optoelectronic properties and device performance to the fabrication processes. In addition to experimental results, simulation techniques have also been applied to predict the optimal morphology, yielding results that are consistent with the experimental conclusion that a nanoscale phase separation with a bicontinuous pathway toward the electrode is desired.[31,32]

Fabrication parameters such as solvent selection and annealing treatment are the most critical factors in film morphology. However, additive incorporation also showed significant benefits toward improving device performance. The overall effects of morphology manipulation assist in forming an interpenetrating network of donor and acceptor molecules, facilitating both charge transfer and carrier transport. Lateral phase separation has been observed and well-understood in several systems. Beyond that, the ingredient distribution of the donor and acceptor molecules along the cross-section of blend films, that is, vertical phase separation, has been observed recently in the nanoscale film morphology, which intuitively governs the charge transport and collection. Thus, an ideal morphology consists of phase separation laterally and vertically, which should both be optimized for satisfying device performance.

This article will focus on recent advances in morphology control, emphasizing on a series of key parameters for film evolution, such as solvent selection and annealing treatment. The concept of using solvent mixtures to manipulate the phase separation process, which enhances the vertical phase separation, will be addressed. As an emerging topic, the second part covers the current status of the inverted-structure polymer solar cells and their advantages when utilizing the spontaneous vertical phase separation. Finally, strategies for further improvement are discussed, with outlooks for future research given.

2. Approaches for Morphology Control of Polymer: Fullerene Bulk Heterojunctions

2.1. Effect of Solvents

Solution processing has many advantages over other film-fabrication technologies, which usually require complicated instruments as well as costly and time-consuming procedures. Therefore, solution processing has developed into the most-favored methodology for fabricating organic optoelectronic devices. Solution processing also allows the freedom to control phase separation and molecular self-organization during solvent evaporation and/or film treatment. The solvent establishes the film evolution environment, and thus has foreseeable impact on the final film morphology. Selection and combination of solvents have been shown to be critical for the morphology in polymer-blend films, and are well-documented in the literature.[33,34] Spin-coating from single-solvent solutions results in thin films, which possess optoelectronic properties determined by the solution parameters and the spin-coating process, for example concentration, blending ratio, spin speed and time, etc. Meanwhile, solvent properties, such as boiling point, vapor pressure, solubility, and polarity, also have considerable impact on the final film morphology. The wettability of the organic solvents on the poly(3,4-ethylenedioxythiophene) poly(styrenesulfonate)

(PEDOT:PSS) surface is usually sufficiently good and not taken into account as a factor on the film morphology. However, it is worth noting that different solution processes have dissimilar requirements for achieving optimal morphology.[35] This article focuses only on the most common spin-coating processes.

In 2001, Shaheen et al. demonstrated the effect of solvent and morphology on device performance for the poly-[2-(3,7-dimethyloctyloxy)-5-methyloxy]-para-phenylene-vinylene (MDMO-PPV):[6,6]-phenyl-C_{61}-butyric acid methyl ester (PCBM) blend system.[36] By replacing toluene with chlorobenzene (CB), the PCE of the device dramatically improved to 2.5%. A more intimate mixing and stronger interchain interaction accounted for this improvement. The solubility of the polymer blend is much better in chlorobenzene than in toluene; thus, a much more uniform mixing of the donor and acceptor is expected. This improved intermixing is evidenced by the roughness of the polymer-blend film, where the chlorobenzene-based sample has a much smoother film surface. Liu et al. investigated the poly(2-methoxy-5-(2′-ethoyl-hexyloxy)-1,4-phenylene vinylene (MEH-PPV):C_{60} blend devices and observed the effect of solvation-induced morphology on device performance.[37] Using nonaromatic solvents, such as tetrahydrofuran (THF) and chloroform, resulted in larger V_{OC} and smaller J_{SC}, due to the fact that MEH-PPV side groups prevented intimate contact and thus efficient charge transfer between the MEH-PPV and C_{60} molecules. Ma et al. also observed that P3HT:PCBM polymer films were smoother and more uniform when chloroform was replaced with CB.[38] The high efficiency is the result of improved morphology, crystallinity, and cathode contact due to better choice of solvent as well as post-annealing treatment.

Because of the better solubility of fullerenes in CB, its use instead of toluene resulted in a finer phase separation, while thermal annealing in both cases led to coarsening of the phases.[39] Figure 1a and b show the scanning electron microscopy (SEM) cross-section views of the MDMO-PPV:PCBM system casted from CB and toluene, respectively. One interesting observation is the 20–40 nm thick "skin" layer observed in the toluene-casted film, in which the PCBM nanocrystallites were generally covered by this "skin" layer, identified as polymer nanospheres. However, for most chlorobenzene-cast films, the polymer nanospheres were homogeneously distributed; therefore, only at very-high PCBM loadings can this phenomenon of PCBM clusters surrounded by a "skin" layer be perceived. The CB-cast films have a finer phase separation and higher J_{SC} in comparison to the toluene-cast films. However, the J_{SC} of CB-cast films decreased with heavier PCBM loadings, indicating that an optimal phase-separated domain size is imperative for good device performance.

Hoppe et al. also measured the localized work function using Kelvin probe force microscopy.[40] CB-cast films showed a uniform work function at the surface but an approximately 0.3 eV decrease upon illumination, while the work function of the toluene-cast films was directly topography-related, increasing in the PCBM clusters under illumination. The work function correlates to the Fermi level, that is, electron density. Under illumination, CB-cast films showed an enrichment of electrons at the surface due to charge generation, while the surface of the toluene-cast films was covered by the polymer skin-layer, causing substantial charge recombination, and a lower J_{SC}. The proposed film morphology and respective charge transport for CB- and toluene-cast films are depicted in Figure 1c and d.

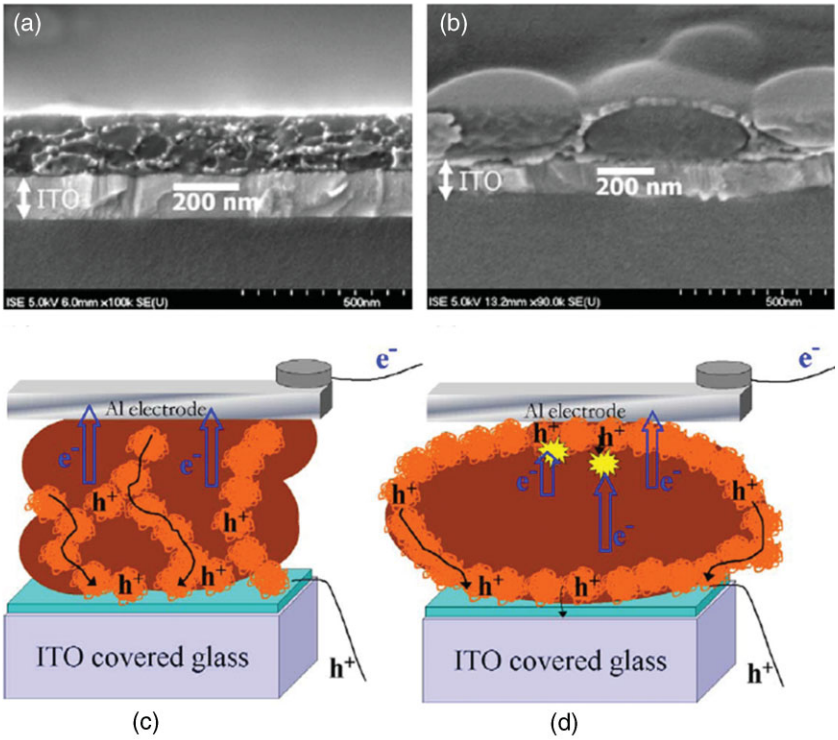

Figure 1. SEM cross-section images of MDMO-PPV:PCBM blend films cast on ITO-glass from a) CB and b) toluene solution. The brighter objects in a) are polymer nanospheres, whereas the darker embedments are PCBM clusters. Schematic of film morphology of c) CB- and d) toluene-cast MDMO-PPV: PCBM blend active layers. In c), carriers form percolated pathways to reach their respective electrodes. In d), electrons and holes suffer from recombination due to undesirable phase separation. Adapted with permission from [40]. Copyright 2006 Elsevier.

The solubility of the fullerene phase can strongly affect the solvent selection. Larger fullerene balls tend to be less soluble, and different solvents have been used for optimal processing conditions. For example, C_{84}-PCBM:MDMO-PPV solar cells were spin-coated from CB and C_{70}-PCBM:MDMO-PPV devices were spin-coated from 1,2-dichlorobenzene (DCB).[23,41] Yao et al. showed that in a new low-band-gap copolymer poly{(9,9-dioctylfluorene)-2,7-diyl-*alt*-[4,7-bis(3-decyloxythien-2-yl)-2,1,3-benzothiadiazole]-5′, 5″-diyl} (PF-*co*-DTB)/C_{70}-PCBM system, DCB resulted in very smooth films (r.m.s. roughness of 0.8 nm) and negligible phase contrast, indicating uniform distribution of the mixture.[25] However, CB produced much rougher films (r.m.s. roughness 4.0 nm) and visible phase separation of 200–300 nm. Based on the exciton diffusion length of approximately 10 nm, CB is not the appropriate solvent for achieving high solar-cell performance in this particular system, and device data also reflected this scenario. It is, however, not sufficient for one to judge the quality of the film merely by the film roughness. In P3HT:PCBM systems, using both thermal annealing and solvent annealing leads to higher roughness than as-cast films, but the device performance in these two cases is much better. The key point is likely to be the formation of proper nanoscale phase separation.

2.2. Effect of Annealing

A variety of post-treatment methods can alter the optoelectronic properties of the polymer-blend films. Annealing processes in polymer solar cells can be divided into two categories: thermal annealing[38,42,43] and solvent annealing.[33,44–46] Both techniques concentrate on improving the nanoscale lateral phase separation of both the crystalline P3HT aggregates and PCBM domains.

Thermal annealing can be applied either on the final device (post-annealing) or on the polymer film only (pre-annealing). The annealing temperature and time are the two most critical parameters in this approach. However, the selection of solvent as well as metal electrodes could also affect the ultimate device performance. In the study of electroluminescence in polythiophene derivatives, Berggren et al. showed that thermal annealing can enhance polymer crystallinity.[47] In 2002, Camaioni et al. reported that thermal treatment at even 55 °C can improve the efficiency of P3HT:fulleropyrrolidine solar cells from 0.1% to 0.6%.[48] Dittmer et al. studied P3HT and a small-molecule dye *N,N′*-bis(1-ethypropyl)-3,4:9,10- perylylene bis(tetracarboxyl diimide) (EP-PTC) system, and observed that thermal annealing at 80 °C for 1 h led to EQE of 11%, an improvement by a factor of 1.6 compared to an untreated device.[49] Padinger's work in 2003 attracted tremendous attention in the field, achieving 3.5% PCE by annealing the RR-P3HT:PCBM blend, which showed that post-annealing and annealing with an external bias are both important.[50] Further extensive studies on the thermal-annealing approach followed, and PCE values up to 5% were reported.[38] Other variations of the thermal annealing also emerged, with one example being the microwave annealing approach reported by Chen et al. in 2007.[51]

The device performance of the polythiophene/fullerene-blend solar cell is critically dependent on the processing condition, which influences the polymer self-organization and the corresponding optical and electrical properties. It has been shown that the crystallinity of P3HT can be increased by thermal annealing, forming crystallites with the conjugated chain parallel to the substrate (*a*-axis orientation).[52] The improved crystallinity enhances the near-infrared (NIR)-region absorption and the hole mobility, and reduces charge recombination due to the improved percolation pathway, all of which led to better device performances. Kim et al. have reported the importance of regioregularity toward P3HT self-organization, as well as increased crystallinity via thermal annealing.[53]

The solvent-annealing approach controls the polymer nanomorphology through the solvent-removal speed. Zhao et al. described a solvent-vapor-annealing approach with similar principles.[54] The benefits of "solvent annealing" have been previously reported by our group.[33,44–46] A systematic study of the spin-coating time reveal the advantage of solvent annealing over thermal annealing by sustaining the P3HT ordered structure upon higher PCBM loadings.[40] The effects of solvent boiling point and film drying time on the polymer crystallinity and absorption were studied by Chu et al. and are illustrated in Figure 2.[55] Controlling the solvent- evaporation rate improved the molecular ordering of the P3HT chains, as was verified by grazing-incidence x-ray diffraction (GIXRD) results in Figure 2a. High-precision synchrotron GIXRD provided clear evidence that the packing of the polymer chain is strongly affected by the solvent-removal rate. Fast solvent removal leads to not only the reduction of P3HT crystallinity, but also increases the interlayer distance of the polymer in the blend film. With carrier transport occuring through a hopping model in the same direction as the interlayer direction, a fast solvent-removal rate is obviously not preferred for polymer solar cells. Figure 2b and c show that solvent annealing is able to enhance the absorption and the EQE in the longer-wavelength region near the band edge of polymers more significantly than thermal annealing alone. The inherent low hole mobility is usually the bottleneck of carrier transport in polymer solar cells, which limits device performance. Various annealing processes can dramatically improve the crystallinity, resulting in higher hole mobility; thus to date annealing has become the most commonly used method for device-performance improvement.

2.3. Effect of Additives

In general, device performance can be improved with post-treatments such as various annealing processes. However, for some material systems, such as the novel low-band-gap polymer poly[2,6-(4,4-bis-(2-ethylhexyl)-4*H*-cyclopenta[2,1-*b*;3,4-*b′*]-dithiophene)-*alt*-4,7-(2,1,3-benzothiadiazole)] (PCPDTBT), which has a better overlap with the solar spectrum, typical post-treatments are incapable of improving the device characteristics.[22,26]

It has been reported that solvent mixtures have a significant effect on film morphology and device performance, namely on J_{SC}, V_{OC}, and *FF* in the polyfluorene copolymer/fullerene system.[56] In the poly(2,7-(9,9-dioctyl-fluorene)-*alt*-5,5-(4′,7′-di-2-thienyl-2′,1′,3-benzothiadiazole)):C_{61}-PCBM blend system, mixing a small volume of CB into chloroform developed a finer and more uniform distribution of domains, which enhanced the J_{SC}. In contrast, adding xylene or toluene into chloroform resulted in larger domain sizes that decreased J_{SC} and caused significant light-intensity-dependent recombination of free charge carriers. Time-resolved spectroscopy on the picosecond scale revealed that charge mobility was considerably improved by adding CB into chloroform, due to an enhanced free-charge-carrier generation from a finer morphology.

Earlier efforts on the solvent-mixture approach concentrated on two miscible solvents, in which both the polymers and fullerenes have considerable solubility. Recently, advances in cooperative effect of solvent mixtures using solvents with distinct solubilities have been obtained.[57,58] The incorporation of additives into a host solvent represents an innovative method and important trend capable of controlling the BHJ morphology. It also provides a unique viewing angle to study the film-formation dynamics of the spin-coating process. However, it is vital to mention that solvent mixtures introduce a more

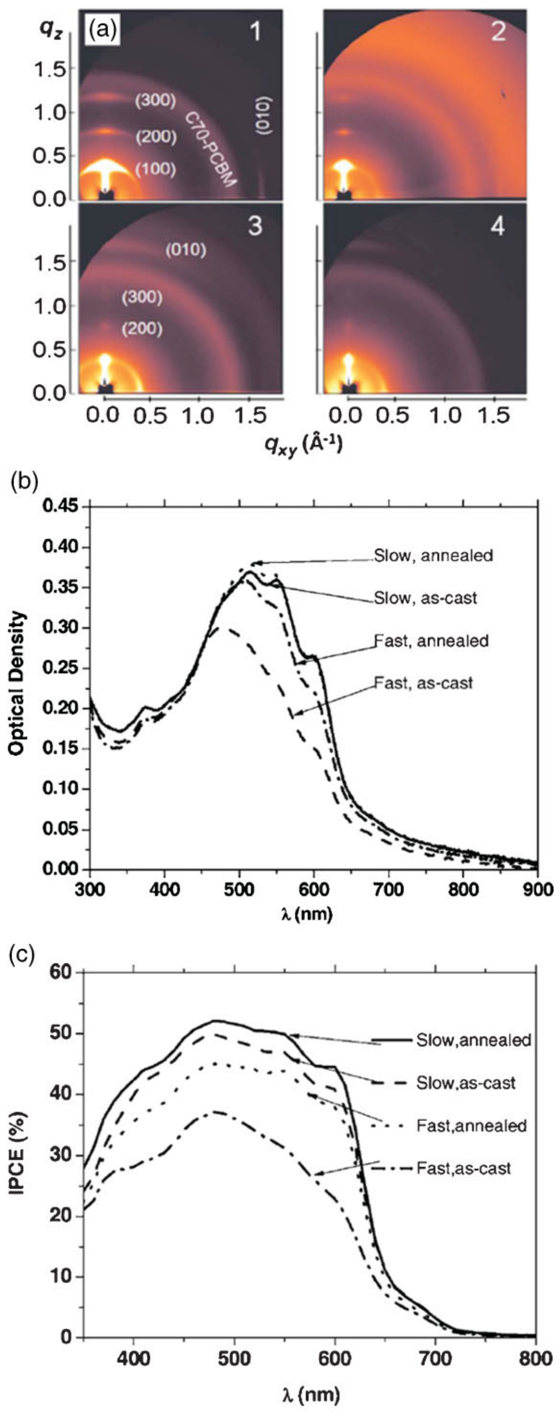

Figure 2. a) 2D GIXRD patterns of RR-P3HT:PC$_{70}$BM (1:1 ratio) films (1) DCB, 1000 rpm, 30 s; 2) DCB, 1000 rpm, 90 s; 3) CB, 1000 rpm, 90 s; 4) CB, 3000 rpm, 90 s). b) UV-vis spectra for RR-P3HT:PC$_{70}$BM (1:1 ratio) films, for fast- and slow-grown films from TCB, before (dash line) and after (solid line) annealing. The films were spun cast at 3000 rpm for 50 s and annealed at 110 °C for 15 min inside the glove box. b) IPCE of RR-P3HT:PC$_{70}$BM solar cells with fast-grown and slow-grown active layers: before (dash line) and after (solid line) annealing. Adapted with permission from [55]. Copyright 2008 American Institute of Physics.

sophisticated circumstance in both the solution and film evolutions, since the solutions now become multicomponent (phase) systems. Therefore, in order to maintain simplicity, only two solvents are usually involved in the solution system when studying the fundamental principles and improving the performance. It should also be noted that the solvent-mixture method should not be restricted to only two solvents; ternary- or even quaternary-solvent systems are also realistic approaches. Recently, the mixture-solvent systems have been intensively explored by several groups, bringing a rather clear understanding of solvent-selection rules for desirable morphology.[57–60]

Previously, the formation of fullerene nanocrystallites by ‘‘bad’’-solvent incorporation was reported by Alargova et al.[61] It was claimed that fullerene molecules tend to crystallize upon contact with a ‘‘bad’’ solvent in order to reduce the overall energy. The narrowly distributed size of these aggregates is proportional to the fullerene concentration and solvent choices, regardless of the volume of the ‘‘bad’’ solvent added. Introduction of alkyl thiols, which are bad solvents for P3HT, to P3HT/PCBM in toluene can increase the photoconductivity and carrier lifetime, due to the enhanced structural order.[24] More recently, Peet et al. reported that by incorporating a few volume percent of alkanedithiols into the PCPDTBT:C$_{71}$-PCBM polymer blend solution, the efficiency doubled from 2.8% to 5.5%, with J_{SC} as high as 16.2 mA cm^{-2}.[57] The vast improvement was attributed to the enhanced interactions between the polymer chains and/or between the polymer and fullerene phases upon alkanedithiol addition, which was evidenced by the absorption data.

A systematic study of alkanedithiol incorporation was carried out by Lee et al. to elucidate the morphology-controlling mechanism, where the alkanedithiols played the role of ‘‘processing additive’’, without reacting with either the polymer or fullerene components.[62] The alkanedithiol selectively dissolved the fullerene phase, while the PCPDTBT was relatively insoluble. Due to the higher boiling points of the alkanedithiols (b.p. >160 °C), the fullerene phase stayed in the solution longer than the polymer, providing more freedom to self-align and crystallize. Consequently, the phase-separation morphology can be manipulated by various alkanedithiols and by tailoring their relative ratios. In addition, the polymer domains are preserved after removal of the fullerene phase, which allowed the direct observation of the exposed polymer network. Figure 3 shows the atomic force microscopy (AFM) and transmission electron microscopy (TEM) images of the PCPDTBT:C$_{71}$-PCBM films with and without 1,8-octanedithiol (OT), as well as the exposed PCPDTBT network after selective dissolution of the C$_{71}$-PCBM. These images clearly show larger PCPDTBT and C$_{71}$-PCBM domains as a result of OT addition, indicating that the improved device performance is related to the better percolating pathways for both carriers from the larger interconnected domains. Carrier-transport analysis also pointed out the enhanced network by the increased electron mobility.[63] Accordingly, two criteria for incorporating alkanedithiols to control the blend-film morphology were proposed: i) selective solubility of the fullerene component and ii) a higher boiling point (lower vapor pressure) than the host solvent. This work provided insight into the mechanism of film-morphology evolution regarding a ‘‘bad’’ solvent addition, and indicated a guideline for alternative solvent-additive selection.

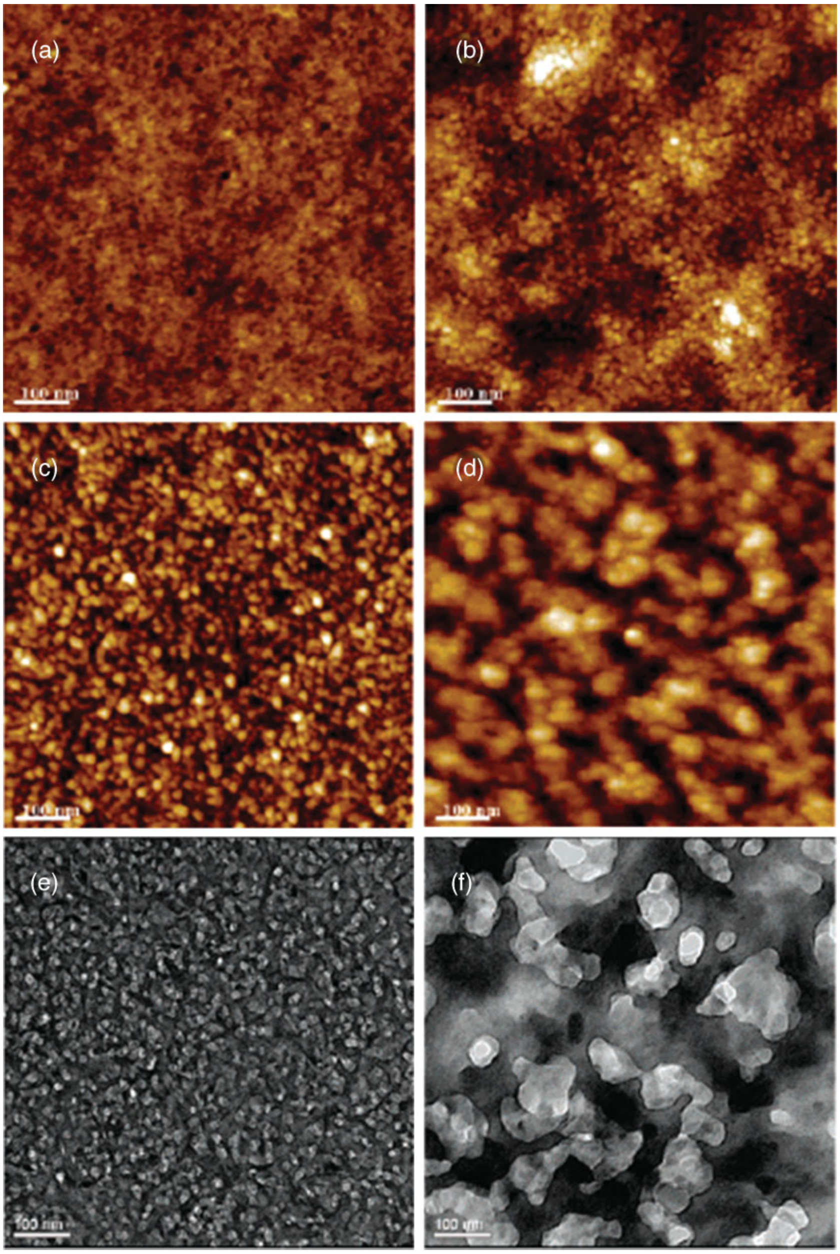

Figure 3. AFM and TEM images of PCPCTBT/C_{71}-PCBM films without and with 1,8-octanedithiol and exposed PCPDTBT networks after removal of C_{71}-PCBM. AFM image of BHJ film a) without and b) with 1,8-octanedithiol. AFM image of exposed polymer networks c) without and d) with 1,8-octanedithiol. TEM image of exposed polymer networks e) without and f) with 1,8-octanedithiol. Adapted with permission from [62]. Copyright 2008 American Chemical Society.

Solution-based titanium oxide (TiO_x) between the active layer and the Al cathode has been demonstrated as an optical spacer via spatially redistributing the optical field within the polymer devices.[64] Principally, the overall absorption of the active layers can be maximized due to better overlap of the optical field with the polymer active layer. The authors claimed that the enhancement of 40% in EQE and 50% in J_{SC} resulted in an overall PCE boost from 2.3 to 5%. However, discrepancy between the experimental results and theoretical prediction indicate the design complexity, where this optical enhancement is only effective in thin active layers.[65] On the other hand, implementing this optical-spacer effect into P3HT:PCBM composites with OT addition is not straightforward.[66] The enhancement in absorption from the optical spacer was compromised by polymer-film surface roughening induced by OT incorporation. Nonetheless, the device performance was still remarkably better than with the incorporation of either of these processes alone. Hawakawa et al. pointed out that the TiO_x layer also acted as a barrier against physical damage and chemical degradation, as well as a hole-blocking layer.[67] Indeed, Kim's result showed an *FF* improvement from 0.54 to 0.66 with the insertion of the TiO_x layer, indicating improved contact at the cathode. Moreover, TiO_x is also well-known as a barrier against oxygen and water diffusion.[68] With the incorporation of the TiO_x layer ($\approx$30 nm) sandwiched between the cathode and polymer layer, air-stable polymer LEDs and solar cells have been demonstrated.[69]

In addition to alkanedithiols, nitrobenzene (NtB) was another mixture solvent recently reported to possess the ability to control the polymer-blend film morphology.[59] It was shown that P3HT exists in both aggregated (crystalline) and amorphous forms in the polymer-blend film, resulting in a multicomponent phase-separated morphology (amorphous P3HT rich and poor in PCBM, and aggregated P3HT rich and poor in PCBM).[70] The ratio of the amorphous-to-aggregated P3HT can be quantitatively analyzed in both the liquid and solid phases according to the solvatochromatic effect. Incorporation of 4.25% NtB in the solution resulted in completely aggregated P3HT in the composite film, with almost 4% PCE for the as-cast device without any post-treatment. Li et al. also demonstrated that by adding a bad solvent for P3HT, hexane, into a well-dissolved P3HT solution, ordered P3HT aggregates could be formed via interchain π–π stacking.[71,72] The preformed ordered P3HT slowly aggregated in the solution and induced the alignment of the P3HT chains, improving the crystallinity and thus conductivity. Similarly, Chen et al. reported that by adding a high-boiling-point solvent, 1-chloronaphthalene (Cl-naph), into the common solvent DCB, the reduced solvent-evaporation rate led to better self-organization of the P3HT chains.[60] The improved crystallinity decreased the series resistance and improved the device efficiency.

Our group also applied this concept to the P3HT:PCBM system, investigating the role of alkanedithiols in the solvent mixtures for the P3HT:PCBM system.[58] OT addition was found to preserve the P3HT crystallinity at heavier PCBM loadings due to the ability to redistribute the P3HT and PCBM phases in the blend film. AFM images revealed a rougher surface for the composite films upon OT addition, with fibrillar crystalline P3HT domains. Using a unique ‘‘float-off’’ method, the top and bottom surface compositions were analyzed by X-ray photoelectron spectroscopy (XPS) without disturbing the film composition, whereas ion-bombardment methods commonly introduce artifacts that alter the film properties.[73,74] XPS analysis reveals an inhomogeneous distribution (vertical phase separation) upon OT addition, where the polymer blend/PEDOT:PSS interface was enriched with PCBM. A PCBM-enriched anode is unfavorable for hole collection in the regular device structure, but is advantageous for the inverted configuration, since the ITO side functions as the cathode instead. A model illustrating the effect of OT incorporation during the spin-coating process was proposed and illustrated in Figure 4. The host solvent DCB has a lower boiling point (198 °C) than OT (270 °C), but a higher solubility for PCBM. As a result, the OT concentration gradually increased during the spin-coating, with PCBM forming clusters and aggregates in the OT phase simultaneously. P3HT has a higher surface energy than PCBM. Thus, in order to reduce the overall energy, P3HT tends to accumulate at the top (air) surface, while PCBM correspondingly segregates at the PEDOT:PSS interface. Accordingly, the preformed PCBM aggregated, and resulting P3HT crystallites formed percolation pathways for both carriers with a favorable vertical phase-separated morphology in the inverted structure. In accordance with the solvent-mixture criteria proposed by Lee, two more additives, di(ethylene glycol)-diethyl ether (DEGDE) and *N*-methyl-2-pyrrolidone (NMP) with similar benefits were also identified. Our work demonstrated a unique method to investigate the buried interface without altering the film properties, and revealed the vertical phase separation of the P3HT:PCBM blend upon ‘‘bad’’-solvent addition. It was pointed out that the inverted configuration might offer a promising alternative to the regular structure by taking advantage of the vertical phase separation. Furthermore, recent studies in our group infer the occurrence of vertical phase separation even without additive incorporation.[75]

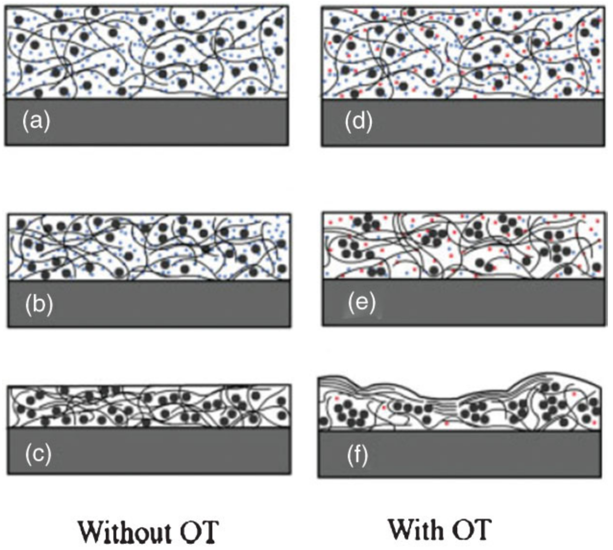

Figure 4. Proposed model of film evolution during the spin-coating process. Black wire: P3HT polymer chain; Large black dots: PCBM; blue dots: DCB molecules; and red dots: 1,8-octanedithiol molecules. a–c) correspond to three stages in the spin-coating process when DCB is the sole solvent; d–f) correspond to three stages in the spin-coating process when octanedithiol is added into DCB. Note the difference of PCBM distribution in the final stage of each case, c) and f). Adapted with permission from [3].

2.4. Vertical Phase Separation

Polymer blends are likely to demix (phase-separate) when spin-coated from blend solutions due to the low entropy of mixing.[76] The rapid quenching of the solvent results in a nonequilibrium morphology; thus film evolution is a rather sophisticated process, in which both thermodynamic and kinetic parameters play substantial roles. The transient bilayer formed by the polymer wetting process is unstable, and subsequently breaks up into lateral domains (dewetting), the sizes of which depend on the solvent-evaporation rate.[77] This morphology evolution was later confirmed by Heriot et al. using time-resolved small-angle light scattering and light reflectivity. It was pointed out that the interface (Marangoni-like) instability was caused by the solvent-concentration gradient in the solidifying film. Budkowski et al. also demonstrated that the solvent-evaporation rate is dependent on the substrate surface chemistry.[78] The polystyrene/polyisoprene (PS/PI) blend spin-coated from toluene onto hydrophilic and hydrophobic SAM-modified substrates formed convex and concave protrusions, respectively, while the overall phase morphology was identical. Walheim et al. reported that by properly tailoring the solvents and substrate surface energy, either component in the immiscible polystyrene/poly (methyl methacrylate) (PS/PMMA) blend can be preferentially segregated at the substrate surface.[79]

In addition to conventional polymers, vertical phase separation has also been reported on a variety of semiconducting polymer-blend systems. Björström et al. utilized dynamic secondary-ion mass spectroscopy (SIMS) and observed a multilayer formation after spin-coating poly [(9,9-dioctylfluorenyl-2,7-diyl)-*co*-5,5-(4′,7′-di-2-thienyl-2′,1′,3′-benzothiadiazole] (APFO-3) blended with PCBM in chloroform.[80] The vertical structure exhibited a four-fold multilayer morphology with APFO-3 enriched at the top surface, followed by a PCBM-enriched layer underneath, then a APFO-3-enriched layer in the middle, and a PCBM-enriched (APFO-3-depleted) adjacent to the silicon substrate. It was suggested that if enough time was allowed for the polymer film to reach thermodynamic equilibrium, a bilayer structure, instead of the frozen four-layer structure, should form. Kim et al. systematically studied poly(2,7-(9,9-di-*n*-octylfluorene-*alt*-benzothiadiazole) (F8BT) and poly(2,7-(9,9-di-*n*-octylfluorene)-*alt*-(1,4-phenylene-((4-*sec*-butylphenyl)imino)-1,4-phenylene)) (TFB) blend using micro-Raman spectroscopy and XPS. An enrichment of the low surface energy component (TFB) at both air and substrate interfaces was observed as a result of interfacial-energy reduction.[81] Furthermore, due to preferential wetting of the hole-transporting TFB layer at the substrate, polymer LEDs without a PEDOT:PSS layer with comparable efficiency were demonstrated. Chappell et al. also reported the preferentially crystallized PFO wetting layer on the surface for a poly(9,9′- dioctylfluorene) (PFO) and poly(9,9′-dioctylfluorene-altbenzothi-adiazole) (F8BT) blend films.[82]

We have investigated the top and bottom surfaces of the polymer active layer and revealed an inhomogeneous distribution of the donor and acceptor material inside the P3HT:PCBM composite films.[58] In fact, vertical phase separation in P3HT:PCBM blends was also previously suggested. Kim et al. attributed the opposite variation of device performance from different solvents (DCB and CB) upon annealing, particularly J_{SC}, to the distinct morphology distribution.[83] It was claimed that the higher boiling point of DCB allowed more time for P3HT to segregate toward the PEDOT:PSS layer, while the rapid evaporation of CB resulted in a more homogeneous distribution. Vertical segregation was also reported in P3HT blended with other semicrystalline polymers, such as polystyrene and polyethylene.[84] The sequential crystallization of both components induced vertical stratification to occur in a "double-percolation-like" mechanism, which was first proposed by Arias et al.[85] The final morphology is the result of successive phase separations, initially in the liquid phase, followed by segregation of the solidified P3HT, which is caused by the crystallization of the matrix component. The exothermic crystallization process provides a driving force for the solidified semiconducting polymer to segregate toward the surfaces and interfaces, resulting in a vertically phase-separated morphology. These vertically stratified structures are beneficial for field-effect-transistor (FET) applications, since transport of charge carriers only takes place at the gate-dielectrics interface. Blended polymer FETs utilizing this concept and using as low as 3 wt% semiconducting polymer were achieved without compromising the performance.

Recently, Campoy-Quiles et al. used variable-angle spectroscopic ellipsometry (VASE) to model the vertical composition profile of P3HT:PCBM thin films cast using various preparation methods.[1] They reported a common vertically and laterally phase-separated morphology, independent of the preparation techniques, which is illustrated in Figure 5. A concentration gradient varying from PCBM-rich near the substrate side to P3HT-rich adjacent to the free (air) surface was observed, regardless of the films cast on fused silica (Fig. 5a) or on PEDOT:PSS-coated fused silica (Fig. 5b). Even after various post-treatments, such as thermal or vapor annealing, the vertical composition profile exhibited similar concentration gradients, but with PCBM protrusions at the surface. Specific substrate treatment was shown to substantially affect the vertical phase-separated morphology. PEDOT:PSS resulted in a slightly less negative concentration gradient than quartz. A hydrophobic self-assembled monolayer (SAM), namely hexamethyldisilazane, was capable of altering the vertical segregation direction, accumulating P3HT at the substrate surface, with PCBM segregating at the air surface, as shown in Figure 5c. Moreover, it was inferred that the morphology evolution was initialized by the crystallization of the P3HT chains followed by diffusion and segregation of PCBM molecules.

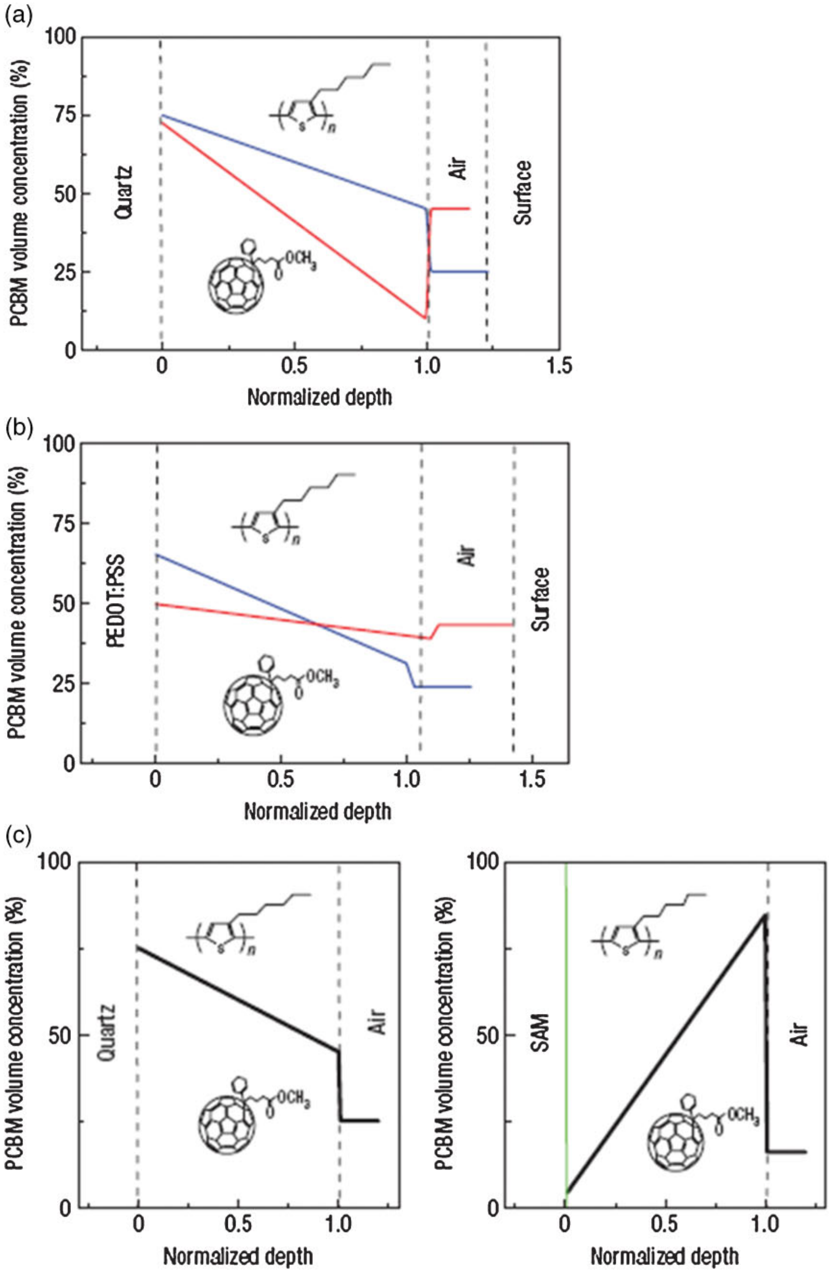

Figure 5. Vertical composition profiles in P3HT:PCBM films as deduced using ellipsometry. a–c) PCBM concentration profiles obtained from analysis of ellipsometric data for P3HT:PCBM blend films: a) spin-coated on fused silica before (blue) and after (red) thermal annealing; b) spin-coated on PEDOT: PSS-coated fused silica before (blue) and after (red) vapor annealing; c) spin-coated on fused silica (left) and on a Si wafer (with native oxide) precoated with a hydrophobic self-assembled hexamethyldisilazane monolayer. Adapted with permission from [1]. Copyright 2008 Nature Publishing Group.

However, recent results from van Bavel et al. indicated dissimilar vertical profiles.[86] By using a novel technique, electron tomography, the three-dimensional phase morphology in nanoscale resolution was imaged. After thermal/solvent annealing, vertical segregation was observed with P3HT nanorods enriched at the bottom surface of the film instead of PCBM crystallites. The vertical segregation was ascribed to the surface-tension difference as well as nucleation sites for P3HT nanorods, provided from the P3HT aggregates.

Several groups have made efforts to realize an ideal morphology in the vertical direction, even though the exact distribution inside the vertical phase-separation morphology is still under debate. Arias et al. have shown that by controlling the solvent-evaporation rate (solvent viscosity) and modifying the substrate surface properties, the vertical phase separation can be tuned to a favorable morphology.[2] In their study, a more viscous solvent (isodurene) is capable of forming a vertical structure instead of lateral domains. Alternatively, using 7-octenyltrichlorosilane (7-OTS) SAMs also formed a favorable segregation of the high-surface-energy component in the polymer blend. Vertical phase separation was confirmed by the observed filter effect via illumination from opposite sides of the device.[87] Upon occurrence of vertical segregation, the EQE should be different with light illuminating from different sides, due to the asymmetric absorption. Indeed, the isodurene-cast films showed a much lower EQE when illuminated from the semitransparent Al cathode, indicating vertical phase separation. Further discussion of other organic electronic applications based on the vertically segregated polymer blends was also reported by Arias.[88] Chen et al. also reported using SAMs to induce vertical segregation.[89] Using microcontact printing (μCP) to pattern 3-aminopropyltriethoxysilane (APTES) SAMs on PEDOT:PSS, an interdigitated structure was obtained by surface-directed phase separation with a more complete phase separation. Absorption data confirmed the improved P3HT alignment, accompanied with a higher hole mobility.

Vertical phase segregation was also observed in hybrid photovoltaics based on CdSe tetrapods and OC_1C_{10}-PPV blends by Sun et al.[90] It was shown that by replacing chloroform with a higher-boiling-point solvent, 1,2,4-trichlorobenzene (TCB), vertical segregation led to an improvement in charge-collection efficiency. Charge collection was more efficienct even with a less efficient charge-dissociation rate due to the coarser phase separation, evidenced by the time-resolved photoluminescence (PL) measurement.

2.5. Summary of Morphology Control

Concluding the results of various works, vertical stratification can be attributed to the different solubilities and surface energies of the blend components as well as the dynamics of the spin-coating process. A volatile solvent is likely to form a more homogeneous film, while a viscous solvent allows vertical phase separation. Upon vertical phase separation, the low-surface-energy component preferentially segregates at the surface or interface to reduce the overall energy. By controlling the film-drying rate via solvent viscosity and spin-coating condition, as well as surface treatment, a closer to optimal, both laterally and vertically segregated morphology can be formed. Furthermore, certain "bad" solvents can function as "processing additives" to preform PCBM aggregates, which assist in the self-organization of both components, and thus induce vertical phase separation. If the vertical segregation can be manipulated to the desired morphology, with a donor-enriched anode and acceptor-enriched cathode, efficient charge dissociation via the interpenetrating network and efficient charge transport along the interconnected pathways are expected to vastly enhance the device performance.

3. Inverted Polymer Solar Cells

3.1. Advantages and Necessity of the Inverted Structure

The regular device structure for polymer solar cells is indium tin oxide (ITO)/PEDOT:PSS/polymer blend/Ca (or LiF)/Al, where a p-type PEDOT:PSS layer is used for anode contact, and a low-work-function metal as the cathode. Both the PEDOT:PSS layer and the low-work-function metal cathode are known to degrade the device lifetime.[91–93] The PEDOT:PSS layer is potentially detrimental to the polymer active layer due to its acidic nature, which etches the ITO and causes interface instability through indium diffusion into the polymer active layer. Low-work-function metals, such as calcium and lithium, are easily oxidized, increasing the series resistance at the metal/BHJ interface and degrading device performance.

In principle, ITO is capable of collecting either holes or electrons, since its work function (≈4.5 to 4.7 eV) lies between the typical highest occupied molecular orbital (HOMO) and lowest unoccupied molecular orbital (LUMO) values of common organic photovoltaic materials. The polarity of the ITO electrode depends mainly on the contact properties, that is, the modification of the ITO surface. For hole extraction, ITO can be coated with a high-work-function layer, such as the PEDOT:PSS layer, which has been proven to form an Ohmic contact with p-type polymer donor materials.[94] On the other hand, Li et al. demonstrated the ability to lower the ITO work function via spin-coating an ultrathin Cs_2CO_3 layer so that ITO becomes the cathode for electron collection.[95] The tunability of the ITO-electrode work function establishes the foundation of an alternative architecture for polymer solar cells, that is, the inverted structure. In the inverted configuration, ITO serves as the cathode, while the anode is built up on the opposite side with a high-work-function electrode.

In the inverted structure, the potential interface instability is overcome by replacing the hole-conducting PEDOT:PSS layer with other functional buffer layers, such as low-work-function alkali compounds to provide the low-work-function contact for ITO.[95,96] On the contrary, the cathode is substituted with either PEDOT:PSS or certain high-work-function transition metal oxides (vanadium oxide (V_2O_5), molybdenum oxide (MoO_3)), covered by a stable metal electrode, such as Au or Ag. These functional buffer layers are ultrathin (a few nm) and highly transparent ($E_g > 3$ eV) to minimize optical losses. As a consequence, the ITO substrate is covered with a low-work-function compound, resulting in the collection of electrons, such that it acts as the cathode. The corresponding high-work-function electrode collects the holes, and serves as the anode. The polarity of the device can thus be controlled by the relative positions of these functional layers with various work functions. Therefore, in the inverted structure, the polarity of the cells can be switched, irrespective of the conducting electrodes.

Besides the improved stability, another motivation for the inverted configuration is to provide design flexibility for tandem[97–101] or stacked cells.[102] Limited absorption in the solar spectrum is the major bottleneck for high PCE, and multiple solar cells in tandem, with distinct absorption spectra, that is, different band-gaps, offer the solution. Nonetheless, for solution-processed polymer solar cells, it is difficult to realize a multilayer structure without dissolution of the layers underneath. The inverted configuration employs a transparent buffer layer, which provides decent protection to the underlying polymer layer against the subsequent solution coating. Consequently, transparent conducting oxides can be deposited without compromising device performance. This provides an efficient method to realize a tandem structure for achieving higher performances.

3.2. Alkali-Metal-Compound Functional Layers Employed in the Inverted Structure

Studies of the inverted configuration have recently arisen, focusing on the functional interfacial layers, and it has been demonstrated for other organic electronic devices, such as light-emitting diodes.[103] Earlier attempts by Sahin et al. tried to mimic that in organic LEDs (OLEDs), and focused on adding layers of functional small-molecule, such as perylene diimide (or bathocuproine (BCP)) and copper phthalocyanine (CuPc), as the electron and hole buffer layers to form inverted polymer solar cells.[93] However, the PCE was merely 0.14%, due to the high series resistance of the organic buffer layers.[104] A few transition metal oxides (V_2O_5, MoO_3) are highly transparent and conductive, and have been demonstrated as efficient anodic buffer layers in polymer solar cells, OLED tandem structures,[105] and organic transistors.[106] Functional interfacial layers at the cathode, such as LiF, have been widely applied in organic and polymer LEDs as well as in solar cells.[107–109] However, the insulating nature of LiF limits the thickness to less than 3 nm for maximum performance, and usually requires to be followed with thermal evaporation of a metal contact to achieve the desired energy-level alignment at the organic/inorganic interfaces.

Cs_2CO_3 is a relatively novel interfacial material, first reported by Canon.[110] In organic LEDs, Cs_2CO_3 is an electron-injection material with the advantage of being insensitive to the contact electrode, and Huang et al. fabricated polymer white-LEDs with 16 lm W^{-1} efficiency incorporating Cs_2CO_3 as the electron-injection layer.[111] By controlling the relative position of V_2O_5 (hole injection) and Cs_2CO_3 (electron injection) layers, a 2.25% PCE inverted polymer solar cell (ITO/Cs_2CO_3/P3HT:PCBM/V_2O_5/Al) was demonstrated.[95] Despite the different work functions for thermally evaporated (2.2 eV) and spin-coated Cs_2CO_3 (3.5 eV) layers, both resulted in comparable device performances for the inverted configuration. Therefore, the polymer/Cs_2CO_3 contact is Ohmic in both cases due to Fermi-level pinning with the LUMO of PCBM.[112] In the conventional regular device structure, inserting 1 nm Cs_2CO_3 between the metal cathode and polymer active layer by thermal evaporation decreases the *J*sc, but increases the V_{OC} and *FF*, indicating possible physical damage or an energy barrier for electron extraction. It has been reported that both thermally evaporated and spin-coated Cs_2CO_3 form an Al–O–Cs complex interfacial layer with Al, which exhibit a very low work function.[113] This low-work-function interface complex is beneficial for electron injection for polymer LEDs, but disadvantageous for electron extraction in photovoltaic devices. However, in the inverted configuration, all device parameters increased with the insertion of the Cs_2CO_3 layer. By replacing the Al top electrode with a semitransparent Au electrode (12 nm), a semitransparent inverted polymer solar cell was fabricated, which should be especially suitable for tandem or stacking cell applications. Solar cells of potentially higher stability can be anticipated with the inert electrodes.

Ouyang et al. reported that by incorporating D-sorbitol into PEDOT:PSS, a transparent electric glue can be formed, which is capable of laminating films together both mechanically and electrically.[114] Implementing the unique electric-glue property of modified PEDOT:PSS into the inverted configuration, a semitransparent polymer solar cell based on P3HT:PCBM blend was fabricated by the lamination process with a 3% PCE.[96] This method took advantage of the solution process and provided an alternative to the roll-to-roll production, which also featured self-encapsulation. Furthermore, a series of alkali metal compounds were evaluated, and revealed the formation of interface dipole layers at the ITO surface, which is shown with the semitransparent device in Figure 6b. As illustrated in Figure 6a, the direction of the dipole moments points from the ITO surface to vacuum, and hence reduces the work function of the ITO surface. The degree of work-function reduction is determined by the magnitude of the dipole moment, which correlates to the V_{OC} variation, and is proportional to the electron-donating ability of the alkali-metal ions.

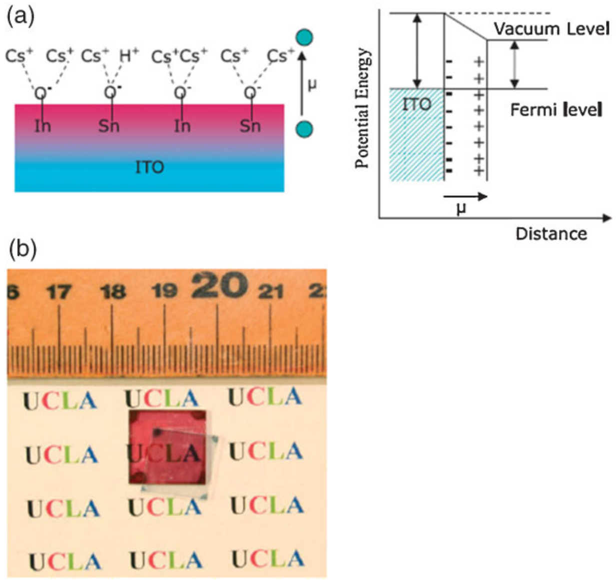

Figure 6. a) Scheme for the formation of dipole layer on ITO and its effect on reducing the work function of ITO. b) Schematic of the semi-transparent laminated device. Adapted with permission from [96]. Copyright 2008, Wiley VCH.

For a regular device configuration, it has been pointed out that the inherent vertical phase separation after spin-coating results in an unfavorable morphology. Nonetheless, this inhomogeneous concentration gradient is favorable for the inverted configuration, since the ITO side, which is the electron-collecting cathode now, is enriched with PCBM. Further discussion on the advantages of the inverted configuration, along with the surface-induced vertical phase separation, follows in the next section.

3.3. Transition Metal Oxide Layers in the Inverted Structure

Besides the alkali metal compounds demonstrated by our group, nanocrystalline and amorphous transition metal oxides, for example ZnO and TiO_x, are solution-processible and also widely applied in optoelectronics because of their low cost and nontoxicity. Moreover, comprehensive research has established solid background knowledge on these two materials. Owing to the large band gaps and matching energy levels, ZnO (work function ~4.3 eV, LUMO ~4.1 eV) and TiO_x (work function ~4.3 eV, LUMO ~4.4 eV) are also suitable functional interfacial layers, since they can block the hole collection on the ITO side, thus inverting the polarity of the devices.

White et al. incorporated a solution-processed ZnO on ITO as the cathode buffer layer with silver as the anode and obtained a PCE of 2.58%.[115] Despite the different configuration, the V_{OC} is similar to those obtained from regular device structures, which can be explained by Fermi-level pinning or dipole formation at the PCBM/ZnO interfaces. Importantly, an EQE maximum of almost 85% was achieved, indicating excellent internal quantum efficiency and overall charge-collection efficiency. The authors attributed the high EQE and J_{SC} to efficient hole collection at the P3HT/Ag interface, which is likely caused by the increased work function of oxidized Ag. However, they also noticed that degradation either in air or in inert environment (desorption of oxygen from ZnO) imposed stability issues on the ZnO-based devices.

Andersen et al. have shown the excellent oxygen-blocking ability of PEDOT:PSS.[116] Therefore, spin-coating the PEDOT:PSS layer above the active layer as the top buffer layer seemed to intuitively improve the stability of the inverted devices. Using ZnO nanoparticles with good electron mobility ($\approx 0.066\,cm^2\,V^{-1}\,s^{-1}$), environmentally stable inverted solar cells were fabricated.[117] A crystalline layer of ZnO nanoparticles (≈50 nm) was formed by the sol–gel process on ITO, and PEDOT:PSS (≈50 nm) was spin-coated on the polymer active layer prior to deposition of the Ag electrode. Inverted cells with an average 3.5% PCE were obtained. Compared to the conventional structure, the J_{SC} and V_{OC} improved due to the additional P3HT/ZnO interface for charge separation and transport. Device stability was substantially improved due to the PEDOT:PSS layer as well as the Ag electrode. The PEDOT:PSS worked as an oxygen-diffusion barrier, while a thin layer of silver oxide increased the effective work function to 5.0 eV, matching that of PEDOT:PSS.

Waldauf et al. used a solution-processed titanium oxide (10 nm) interlayer as the electron-selective contact and PEDOT:PSS/Au as the anode to form an inverted polymer solar cell.[118] Due to the hydrophobicity of the polymer active layer, the PEDOT:PSS solution was diluted in isopropanol and preheated at 80 °C prior to spin-coating. Using *o*-xylene as the solvent led to a 25 times higher hole mobility than electron mobility and less vertical phase separation, with a 3.1% PCE. Compared to the conventional structure, the inverted cell showed a lower current in both the forward- and reverse-bias direction. The lower current under forward bias was caused by the higher series resistance from the TiO_x layer, while the lower leakage current under reverse bias can be attributed to the effective hole-blocking TiO_x layer. In a previous study using CB as the solvent, the J_{SC} of the inverted configuration was only half of the regular structure.[119] Accordingly, it was claimed that CB formed a favorable vertical phase separation for the regular structure, with P3HT accumulated adjacent to the PEDOT:PSS layer. In contrast, using *o*-xylene resulted in comparable J_{SC} and PCE; hence, it was speculated that *o*-xylene formed a favorable morphology in the inverted configuration, where less vertical phase separation was induced or even a composition gradient with P3HT-enriched at the PEDOT:PSS side and PCBM-enriched at the TiO_x side could be formed.

Inserting an ultrathin layer of polyoxyethylene tridecyl ether (PTE) between the charge-selective TiO_x layer and the ITO substrate significantly improved the wetting of the TiO_x precursor.[120] The more-uniform TiO_x layer thus formed a better contact, with a higher *FF* due to reduced series resistance and increased shunt resistance, resulting an overall PCE of 3.6%.

Ameri et al. were the first to carry out optical modeling to compare the regular and inverted structures.[121] The inverted device showed an EQE maximum approximately 11% higher than the regular devices (75% vs. 64%). The active layer in the regular configuration absorbed less photons due to the absorption losses from the PEDOT:PSS layer.[122] Moreover, no significant "optical spacer" effect was observed for various thicknesses of the TiO_x or PEDOT:PSS layers for the inverted structure.

In addition to the hole-blocking ability, TiO_2 has also been reported to exhibit efficient photoinduced electron transfer from conjugated polymers into TiO_2.[123,124] After the initial reports of efficient charge transfer from dyes to TiO_2, the basis of dye-sensitized solar cells,[125] preliminary reports of hybrid TiO_2–polymer photovoltaic devices with bilayer,[126] nanostructured,[127–129] or blended architecture[130,131] have been successfully demonstrated. In this article, only the nanostructured hybrid TiO_2–polymer photovoltaic device will be discussed, because of its relevancy to the inverted configuration. A more detailed review on hybrid polymer–metal oxide photovoltaics can be found in the article by Bouclé et al.[132]

It has been proposed that an ordered heterojunction provides a straightforward pathway for electron collection by utilizing the mesostructured TiO_2, which is infiltrated with a donor material.[133] The ordered heterojunction offers several advantages, such as controlled nanoscale phase separation of both phases, straight pathways without dead ends, and easy modeling for further understanding. McGehee et al. demonstrated hybrid P3HT–titania ordered BHJ photovoltaic devices with PCE approximately 0.5%. The efficiency was limited by the poor alignment (crystallization) and low mobility, as well as insufficient infiltration of the polymer. Recently, Mor et al.[134] demonstrated an efficient double-heterojunction polymer solar cell via vertically oriented TiO_2 nanotube arrays, with PCE

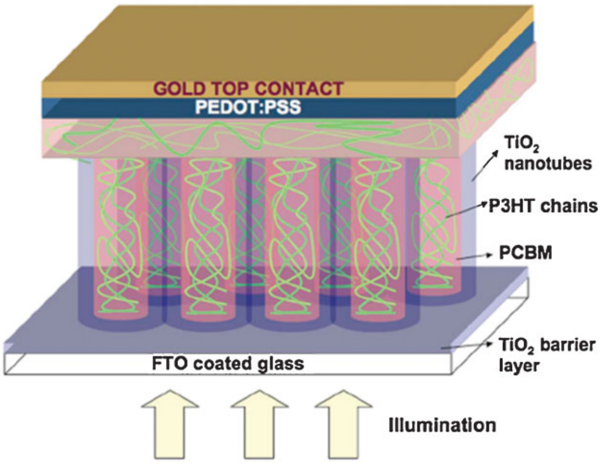

Figure 7. Illustration showing the TiO_2-nanotube inverted device configuration. Adapted with permission from [134]. Copyright 2007 American Institute of Physics.

approaching 4.1%. The device structure is illustrated in Figure 7. By tailoring the pore sizes of the TiO_2 nanotubes, the infiltrated polymer chains self-aligned into aggregates according to the nanotube direction. Coakley et al. also reported that the hole mobility can be enhanced 20 times by this vertical channel-confinement-induced alignment.[135] Moreover, both polymer–fullerene and polymer–TiO_2 interfaces provided efficient charge separation, and the nanotube arrays prevented charge recombination at the electrodes, since contact with both electrodes simultaneously was avoided as well. This double-heterojunction device exhibited an EQE maximum of 80%, and an excellent J_{SC} of 12.4 mA cm^{-1}. Similarly, Takanezawa et al. also reported 2.7% PCE double-heterojunction devices utilizing ZnO-nanorod arrays with the P3HT:PCBM system.[136]

4. Strategies and Outlook

4.1. Strategies to Improve the Performance of Inverted-Structure Polymer Solar Cell

Table 1 summarizes the device characteristics of some representative results regarding the inverted structure polymer solar cells. One key factor for improving the device performance of the inverted polymer solar cells is to reduce the series resistance, particularly the resistance of the functional buffer layer. It is well known that a high series resistance can be reflected by the significant reduction in J_{SC} and FF. The group from Konarka showed that the inverted structure benefited from a reduced optical loss due to the non-negligible PEDOT:PSS layer, and also from the improved contact of the ITO/PTE/TiO_x cathode.[120,121] Recently, we considerably improved the device performance of the inverted structure polymer solar cell from 2.3 to 4.2% PCE by annealing the spin-coated Cs_2CO_3 functional buffer layer.[137] This efficiency is so far the highest PCE demonstrated for the inverted configuration, and is comparable to the regular structure based on the same system and similar process conditions. This significantly narrowed the gap between regular and inverted structure solar cells, providing a promising alternative for structure design flexibility. The device performance (current–voltage characteristics) versus annealing temperature of the Cs_2CO_3 functional layer are shown in Figure 8a, and the significant device improvement is attributed to the reduced interfacial resistance at the cathode. Figure 8b reveals the variation of the PCE and the Cs_2CO_3 surface property with the annealing temperature via contact angle with water. The inset in Figure 8b shows the effect of annealing treatment on EQE. Line I is Cs_2CO_3 layer without annealing, and line II is after 150 °C annealing. It has been suggested that Cs_2CO_3 decomposes into stoichiometric Cs_2O doped with Cs_2O_2 during thermal evaporation.[113,137,138] The doped cesium oxide behaves as an n-type semiconductor, with a lower interface resistance than pristine Cs_2CO_3, as well as having a relatively low work function.

The best regular P3HT:PCBM device fabricated in our lab so far exhibited a 4.4% PCE, which was slightly higher than our newly reported inverted device. It is believed that the inverted device benefited from the spontaneous vertical phase separation, with a higher EQE maximum (72 compared to 63%) and J_{SC} (11.13 vs. 10.6 mA cm^{-2}) in comparison to the regular configuration. However, the overall device performance is slightly inferior, due to a lower V_{OC} and FF. Figure 9 compares the EQE of the regular- and inverted-device structures. The inverted structure showed a higher EQE over the whole absorption spectra, while no difference was observed from the UV-vis absorption results. Thus, the spontaneous vertical phase separation of the P3HT:PCBM blend results in a P3HT-enriched top surface, and a PCBM-enriched bottom contact, which accounts for the enhanced charge-collection efficiency. The vertical phase separation suggested improved charge-collection efficiency due to the favored distribution of the donor and acceptor materials within the polymer blend. As a consequence, the electrode selectivity can be substantially improved, because less charge recombination is expected from the accumulation of the donor and acceptor

Table 1. Summarized results of the device characteristics from representative inverted polymer solar cells.

Device structure	J_{SC} [mA cm^{-2}]	V_{OC} [V]	FF [%]	PCE [%]	Reference
ITO/Cs_2CO_3/P3HT:PCBM/V_2O_5/Al	8.42	0.56	62.1	2.25	95
ITO/ZnO/P3HT:PCBM/Ag	11.22	0.556	47.5	2.58	115
ITO/TiO_x/P3HT:PCBM/PEDOT:PSS/Au	9.0	0.56	62	3.10	119
ITO/PTE/TiO_x/P3HT:PCBM/PEDOT:PSS/Ag	10.2	0.56	64	3.60	120
ITO/ZnO NP/P3HT:PCBM/PEDOT:PSS/Ag	11.17	0.623	54.3	3.30	117
FTO/TiO_2/P3HT:PCBM/PEDOT:PSS/Au	12.40	0.641	51.1	4.07	134
ITO/annealed-Cs_2CO_3/P3HT:PCBM/V_2O_5/Al	11.13	0.59	63	4.19	137

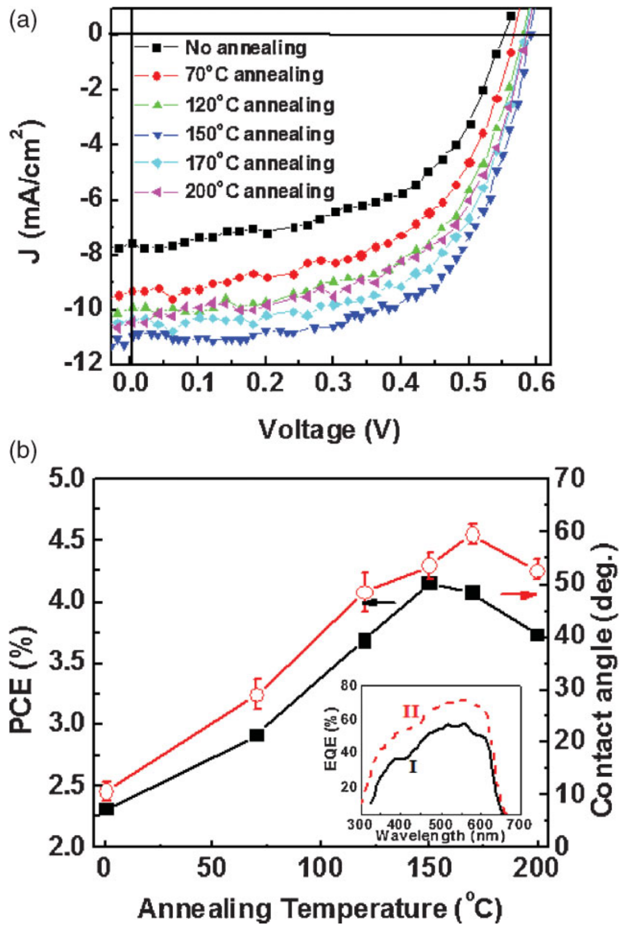

Figure 8. a) *I*–*V* characteristics of the inverted PV devices under illumination with various annealing temperatures of the Cs_2CO_3 layer. b) PCE and contact angle with water of the Cs_2CO_3 layer as a function of different annealing temperatures. The inset in b) shows the effect of annealing treatment on the EQE. Line I is Cs_2CO_3 layer without annealing, and line II is after 150 °C annealing. Adapted with permission from [137]. Copyright 2007 American Institute of Physics.

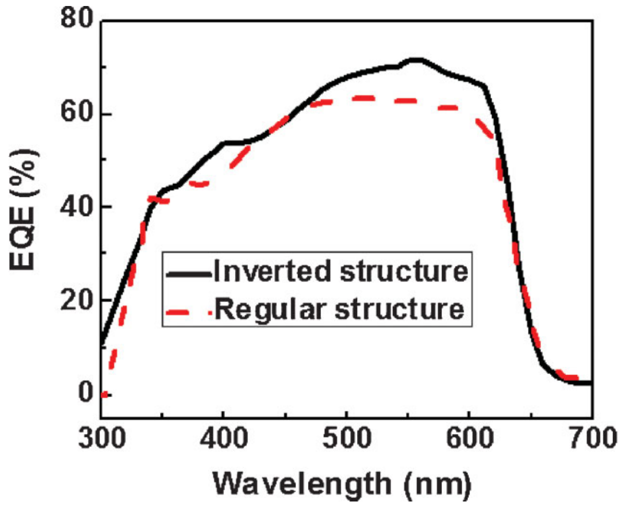

Figure 9. External quantum efficiency of the regular and inverted device structure based on P3HT: PCBM blend.

materials at the anode and cathode, respectively. Indeed, EQE maximums exceeding 80% based on the inverted structure have been reported, while this number has not yet been obtained for the regular device structure.[115,134] Further improvement of the inverted configuration can still be expected by optimizing the energy alignment between the polymer/electrode interfaces and further increasing the conductivity of the functional buffer layers.

The inverted structure also bears resemblance to the hybrid planar-mixed molecular heterojunction in organic small-molecule solar cells, where an interdiffused layer of donor–acceptor materials is sandwiched between the donor and acceptor layers, thus combining the advantages of both the bilayer and bulk-heterojunction structures.[139] A 5% PCE was achieved using the structure ITO/CuPc/CuPc:C_{60}/C_{60}/BCP/Ag, where the mixed-layer CuPc:C_{60} was attained by coevaporation. However, in polymer solar cells such distribution is difficult to realize. Although previous efforts by partially dissolving the polymer to form a stratified multilayer of donor–acceptor blends have been demonstrated, only a PCE of 0.5% was achieved.[140]

Recently, Wei et al. synthesized a new fullerene derivative with a fluorocarbon chain (F-PCBM), and blended into P3HT:PCBM solution.[141] F-PCBM preferentially segregates a layer 2 nm thick at the top surface due to the lower surface energy from the fluorinated side groups.[142] Via this approach, the *FF* increased to an impressively high 72%, and was mainly attributed to the surface dipole moment induced by the F-PCBM layer, which decreased the energy barrier between the Al cathode and the PCBM. Nonetheless, this device structure demonstrated an ideal vertical phase separation, with the electron-acceptor material enriched adjacent to the cathode. A sufficiently large interfacial area was obtained from the bulk-heterojunction structure, while the cathode was intentionally enriched with an electron-acceptor layer, reducing possible charge recombination with the donor. Other polymer-based electronics with excellent exciton dissociation and charge transport characteristics have been fabricated via the lamination process, where a bilayer polymer structure was formed with an excellent interpenetrating network.[143,144]

It has been shown that vertical stratification of the polymer-blend film is a rather spontaneous process in addition to the lateral phase separation. However, several examples have demonstrated that control of the vertical distribution of individual components can be achieved by carefully manipulating the spin-casting parameters, such as solubility, surface energy, and solvent viscosity. Furthermore, recent work on solvent mixtures also provided a novel approach to ''intelligently'' achieve an optimized morphology, and the clear comprehension of the underlying mechanism should pave the path toward better device performance.[3]

4.2. Outlook

Morphology control crucially remains the core issue to achieve high performance for polymer solar cells. An ideal morphology consists of nanoscale phase separation, with an interpenetrating network of the two separate phases for efficient exciton dissociation. The bulk-heterojunction phase separation should form aggregated donor and acceptor domains, in which their sizes are comparable to the exciton diffusion length. Meanwhile, a bicontinuous percolation path should be formed for maximal charge extraction from the polymer active layer with a donor-enriched anode and acceptor-enriched cathode. Encounter of opposite-charged carriers results in nongeminated recombination losses, thus a larger domain size leads to higher carrier mobility, which ensures instant carrier extraction rather than forming space charges. Under this scenario, improved mobility and reduced recombination facilitate charge transport and extraction/injection. In terms of J–V characteristics, this improvement corresponds to larger shunt resistances and smaller series resistances, leading to an increased *FF* and eventually high efficiency. As a consequence, the trade-off between a percolation pathway and optimal domain size becomes the key factor for achieving high efficiency.

In cases where vertical phase separation occurs for polymer/fullerene blends, this spontaneous inhomogeneous composition profile is favorable for the inverted structure, where an EQE maximum approaching unity can be expected. Similar to regular structures, electrodes must have strict selectivity for charge extraction. Matching of work functions of both electrodes with the transporting levels of bulk heterojunctions is important to maximize the V_{OC}, and it is desirable to develop multiple approaches to modify the work function of the electrodes. The nanostructure and surface energy of the n-type materials on the cathode side, such as Cs_2CO_3, ZnO, and TiO_x, play important roles in forming a desirable film morphology and interface contact. The p-type anode buffer layer must present a suitable work function for efficient hole collection as well as high conductivity and low absorption throughout the UV-vis-NIR range to maximize effective absorption. Meanwhile, separating the active layer from the anode reduces quenching and diffusion effects induced by the metal layer, which degrade both efficiency and stability. Since the p-type layers usually have work functions of around 5.0 eV, it can also serve as a protection layer against oxygen and moisture, which are also among major causes of degradation.

The inherent vertical phase separation, combined with the improved stability, makes the inverted configuration an appealing alternative to the conventional regular structure, and also provides design flexibility for tandem-cell design. Therefore, the advantage of the inverted structure in polymer-film morphology evolution is identified, and it can be extended beyond the P3HT:PCBM system. Manipulation of film morphology via vertical phase separation and utilization of the inverted structure allow us to derive a general structure-design rule for future material systems for polymer photovoltaic application.

Acknowledgements

The authors acknowledge the useful discussions of various topics with Dr. Y. Yao and Dr. H.-H. (Joseph) Liao. Financial support from Solarmer Energy Inc., University of California Discovery Grant, and NSF IGERT: Materials Creation Training Program (MCTP) (DGE-0114443) and the California Nano-Systems Institute are acknowledged. This article is part of a Special Issue on Interfaces in Organic Electronics.

Received: September 26, 2008
Revised: November 25, 2008

---

[1] M. Campoy-Quiles, T. Ferenczi, T. Agostinelli, P. G. Etchegoin, Y. Kim, T. D. Anthopoulos, P. N. Stavrinou, D. D. C. Bradley, J. Nelson, *Nat. Mater.* **2008**, *7*, 158.
[2] A. C. Arias, N. Corcoran, M. Banach, R. H. Friend, J. D. MacKenzie, W. T. S. Huck, *Appl. Phys. Lett.* **2002**, *80*, 1695.
[3] Y. Yan, J. H. Hou, Z. Xu, G. Li, Y. Yang, *Adv. Funct. Mater.* **2008**, *18*, 1783.
[4] C. K. Chiang, J. C. R. Fincher, Y. W. Park, A. J. Heeger, H. Shirakawa, E. J. Louis, *Phys. Rev. Lett.* **1977**, *39*, 1098.
[5] H. Shirakawa, E. J. Louis, A. G. MacDiarmid, C. K. Chiang, A. J. Heeger, *J. Chem. Soc. Chem. Commun.* **1977**, 578.
[6] H. Tomozawa, D. Braun, S. Phillips, A. J. Heeger, H. Kroemer, *Synth. Met.* **1987**, *22*, 63.
[7] C. W. Tang, S. A. VanSlyke, *Appl. Phys. Lett.* **1987**, *51*, 913.
[8] J. H. Burroughes, D. D. C. Bradley, A. R. Brown, R. N. Marks, K. Mackay, R. H. Friend, P. L. Burns, A. B. Holmes, *Nature* **1990**, *347*, 539.
[9] G. Gustafsson, Y. Cao, G. M. Treacy, F. Klavetter, N. Colaneri, A. J. Heeger, *Nature* **1992**, *357*, 477.
[10] C. W. Tang, *Appl. Phys. Lett.* **1986**, *48*, 183.
[11] G. Yu, A. J. Heeger, *J. Appl. Phys.* **1995**, *78*, 4510.
[12] J. J. M. Halls, C. A. Walsh, E. A. Marseglia, R. H. Friend, S. C. Moratti, A. B. Holmes, *Nature* **1995**, *376*, 498.
[13] H.-Y. Chen, M. K. F. Lo, G. Yang, H. G. Monbouquette, Y. Yang, *Nat. Nanotechnol.* **2008**, *3*, 543.
[14] J. H. Burroughes, C. A. Jones, R. H. Friend, *Nature* **1988**, *335*, 137.
[15] F. Garnier, R. Hajlaoui, A. Yasser, P. Srivastava, *Science* **1994**, *265*, 1684.
[16] Y. Yang, A. J. Heeger, *Nature* **1994**, *372*, 344.
[17] L. Torsi, A. Dodabalapur, L. J. Rothberg, A. W. P. Fung, H. E. Katz, *Science* **1996**, *272*, 1462.
[18] L. Ma, J. Liu, Y. Yang, *Appl. Phys. Lett.* **2002**, *80*, 2997.
[19] J. Ouyang, C.-W. Chu, C. R. Szmanda, L. Ma, Y. Yang, *Nat. Mater.* **2004**, *3*, 918.
[20] Y. Yang, L. Ma, J. Wu, *MRS Bull.* **2004**, *29*, 833.
[21] R. J.-H. Tseng, J. Huang, J. Ouyang, R. B. Kaner, Y. Yang, *Nano Lett.* **2005**, *5*, 1077.
[22] D. Mühlbacher, M. Scharber, M. Morana, Z. Zhu, D. Waller, R. Gaudiana, C. J. Brabec, *Adv. Mater.* **2006**, *18*, 2884.
[23] F. B. Kooistra, V. D. Mihailetchi, L. M. Popescu, D. Kronholm, P. W. M. Blom, J. C. Hummelen, *Chem. Mater.* **2006**, *18*, 3068.
[24] J. Peet, C. Soci, R. C. Coffin, T. Q. Nguyen, A. Mikhailovsky, D. Moses, G. C. Bazan, *Appl. Phys. Lett.* **2006**, *89*, 252105.
[25] Y. Yao, C. Shi, G. Li, V. Shrotriya, Q. Pei, Y. Yang, *Appl. Phys. Lett.* **2006**, *89*, 153507.
[26] C. Soci, I.-W. Hwang, D. Moses, Z. Zhu, D. Waller, R. Gaudiana, C. J. Brabec, A. J. Heeger, *Adv. Funct. Mater.* **2007**, *17*, 632.
[27] E. Wang, L. Wang, L. Lan, C. Luo, W. Zhuang, J. Peng, Y. Cao, *Appl. Phys. Lett.* **2008**, *92*, 033307.
[28] J. Hou, H.-Y. Chen, S. Zhang, G. Li, Y. Yang, *J. Am. Chem. Soc.* **2008**, *130*, 16144.
[29] K. Emery, in *Handbook of Photovoltaic Science and Engineering* (Eds: A, Luque, S. Hegedus), Wiley-VCH, Weinheim, Germany **2003**, Ch. 16.
[30] V. Shrotriya, G. Li, Y. Yao, Y. Yang, T. Moriarty, K. Emery, *Adv. Funct. Mater.* **2006**, *16*, 2016.
[31] B. Lei, Y. Yao, A. Kumar, Y. Yang, V. Ozolins, *J. Appl. Phys.* **2008**, *104*, 024504.
[32] P. Watkins, A. Walker, G. Verschoor, *Nano Lett.* **2005**, *5*, 1814.
[33] G. Li, V. Shrotriya, Y. Yao, J. Huang, Y. Yang, *J. Mater. Chem.* **2007**, *17*, 3126.
[34] H. Hoppe, N. S. Sariciftci, *J. Mater. Chem.* **2006**, *16*, 56.
[35] C. N. Hoth, P. Schilinsky, S. A. Choulis, C. J. Brabec, *Nano Lett.* **2008**, *8*, 2806.
[36] S. E. Shaheen, C. J. Brabec, N. S. Sariciftci, F. Padinger, T. Fromherz, J. Hummelen, *Appl. Phys. Lett.* **2001**, *78*, 841.
[37] J. Liu, Y. Shi, Y. Yang, *Adv. Funct. Mater.* **2001**, *11*, 1.

[38] W. Ma, C. Yang, A. J. Heeger, *Adv. Funct. Mater.* **2005**, *15*, 1617.
[39] H. Hoppe, M. Niggemann, C. Winder, J. Kraut, R. Hiesgen, A. Hinsch, D. Meissner, N. S. Sariciftci, *Adv. Funct. Mater.* **2004**, *14*, 1005.
[40] H. Hoppe, T. Glatzel, M. Niggemann, W. Schwinger, F. Schaeffler, A. Hinsch, M. Ch, Lux-Steiner, N. S. Sariciftci, *Thin Solid Films* **2006**, *511*, 587.
[41] M. M. Wienk, J. M. Kroon, W. J. H. Verhees, J. Knol, J. C. Hummelen, P. A. van Hal, R. A. J. Janssen, *Angew. Chem. Int. Ed.* **2003**, *42*, 3371.
[42] G. Li, V. Shrotriya, Y. Yao, J. Huang, Y. Yang, *J. Appl. Phys.* **2005**, *98*, 043704.
[43] V. D. Mihailetchi, H. X. Xie, B. de Boer, L. J. A. Koster, P. W. M. Blom, *Adv. Funct. Mater.* **2006**, *16*, 699.
[44] G. Li, Y. Yao, H. Yang, V. Shrotriya, G. Yang, Y. Yang, *Adv. Funct. Mater.* **2007**, *17*, 1636.
[45] V. Shrotriya, Y. Yao, G. Li, Y. Yang, *Appl. Phys. Lett.* **2006**, *89*, 063505.
[46] G. Li, V. Shrotriya, J. Huang, Y. Yao, T. Moriarty, K. Emery, Y. Yang, *Nat. Mater.* **2005**, *4*, 864.
[47] M. Berggren, G. Gustafsson, O. Inganas, M. R. Andersson, O. Wennerstrom, T. Herberg, *Appl. Phys. Lett.* **1994**, *65*, 1489.
[48] N. Camaioni, G. Ridolfi, G. Casalbore-Miceli, G. Possamai, M. Maggini, *Adv. Mater.* **2002**, *14*, 1735.
[49] J. J. Dittmer, E. A. Marseglia, R. H. Friend, *Adv. Mater.* **2000**, *12*, 1270.
[50] F. Padinger, R. S. Rittberger, N. S. Sariciftci, *Adv. Funct. Mater.* **2003**, *13*, 85.
[51] C.-J. Ko, Y.-K. Lin, F.-C. Chen, *Adv. Mater.* **2007**, *19*, 3520.
[52] T. Erb, U. Zhokhavets, G. Gobsch, S. Raleva, B. Stühn, P. Schilinsky, C. Waldauf, C. J. Brabec, *Adv. Funct. Mater.* **2005**, *15*, 1193.
[53] Y. Kim, S. Cook, S. M. Tuladhar, S. A. Choulis, J. Nelson, J. R. Durrant, D. D. C. Bradley, M. Giles, I. McCulloch, C.-S. Ha, M. Ree, *Nat. Mater.* **2006**, *5*, 197.
[54] Y. Zhao, Z. Xie, Y. Qu, Y. H. Geng, L. X. Wang, *Appl. Phys. Lett.* **2007**, *90*, 043504.
[55] C.-W. Chu, H. Yang, W.-J. Hou, J. Huang, G. Li, Y. Yang, *Appl. Phys. Lett.* **2008**, *92*, 103306.
[56] F. Zhang, K. G. Jespersen, C. Björström, M. Svensson, M. R. Andersson, V. Sundström, K. Magnusson, E. Moons, A. Yartsev, O. Inganäs, *Adv. Funct. Mater.* **2006**, *16*, 667.
[57] J. Peet, J. Y. Kim, N. E. Coates, W. L. Ma, D. Moses, A. J. Heeger, G. C. Bazan, *Nat. Mater.* **2007**, *6*, 497.
[58] Y. Yao, J. H. Hou, Z. Xu, G. Li, Y. Yang, *Adv. Funct. Mater.* **2008**, *18*, 1783.
[59] A. J. Moulé, K. Meerholz, *Adv. Mater.* **2008**, *20*, 240.
[60] F.-C. Chen, H.-C. Tseng, C.-J. Ko, *Appl. Phys. Lett.* **2008**, *92*, 103316.
[61] R. G. Alargova, S. Deguchi, K. Tsujii, *J. Am. Chem. Soc.* **2001**, *123*, 10460.
[62] J. K. Lee, W. L. Ma, C. J. Brabec, J. Yuen, J. S. Moon, J. Y. Kim, K. Lee, G. C. Bazan, A. J. Heeger, *J. Am. Chem. Soc.* **2008**, *130*, 3619.
[63] I.-W. Hwang, S. Cho, J. Y. Kim, K. Lee, N. E. Coates, D. Moses, A. J. Heeger, *J. Appl. Phys.* **2008**, *104*, 033706.
[64] J. Y. Kim, S. H. Kim, H.-H. Lee, K. Lee, W. Ma, X. Gong, A. J. Heeger, *Adv. Mater.* **2006**, *18*, 572.
[65] J. Gilot, I. Barbu, M. M. Wienk, R. A. J. Janssen, *Appl. Phys. Lett.* **2007**, *91*, 113520.
[66] J. K. Lee, N. E. Coates, S. Cho, N. S. Cho, D. Moses, G. C. Bazan, K. Lee, A. J. Heeger, *Appl. Phys. Lett.* **2008**, *92*, 243308.
[67] A. Hayakawa, O. Yoshikawa, T. Fujieda, K. Uehara, S. Yoshikawa, *Appl. Phys. Lett.* **2007**, *90*, 163517.
[68] A. L. Linsebigler, G. Lu, J. T. Yates, *Chem. Rev.* **1995**, *95*, 735.
[69] K. Lee, J. Y. Kim, S. H. Park, S. H. Kim, S. Cho, A. J. Heeger, *Adv. Mater.* **2007**, *19*, 2445.
[70] J. K. J. van Duren, X. N. Yang, J. Loos, C. W. T. Bulle-Lieuwma, A. B. Sieval, J. C. Hummelen, R. A. J. Janssen, *Adv. Funct. Mater.* **2004**, *14*, 425.
[71] L. G. Li, G. H. Lu, X. N. Yang, *J. Mater. Chem.* **2008**, *18*, 1984.
[72] S. D. D. V. Rughooputh, S. Hotta, A. J. Heeger, F. Wudl, *J. Polym. Sci. Part B* **1987**, *25*, 1071.
[73] A. Turak, D. Grozea, X. D. Feng, Z. H. Lu, H. Aziz, A. M. Hor, *Appl. Phys. Lett.* **2002**, *81*, 766.
[74] S. G. MacKay, M. Bakir, I. H. Musselman, T. J. Meyer, R. W. Linton, *Anal. Chem.* **1991**, *63*, 60.
[75] Z. Xu, L.-M. Chen, G. Yang, C.-H. Huang, J. Hou, Y. Wu, G. Li, C.-S. Hsu, Y. Yang, *Adv. Funct. Mater.* in press.
[76] M. Geoghegan, G. Krausch, *Prog. Polym. Sci.* **2003**, *28*, 261.
[77] S. Y. Heriot, R. A. L. Jones, *Nat. Mater.* **2005**, *4*, 782.
[78] A. Budkowski, A. Bernasik, P. Cyganik, J. Raczkowska, B. Penc, B. Bergues, K. Kowalski, J. Rysz, J. Janik, *Macromolecules* **2003**, *36*, 4060.
[79] S. Walheim, M. Böltau, J. Mlynek, G. Krausch, U. Steiner, *Macromolecules* **1997**, *30*, 4995.
[80] C. M. Björström, A. Bernasik, J. Rysz, A. Budkowski, S. Nilsson, M. Svensson, M. R. Andersson, K. O. Magnusson, E. Moons, *J. Phys. Condens. Matter* **2005**, *17*, L529.
[81] J.-S. Kim, P. K. H. Ho, C. E. Murphy, R. H. Friend, *Macromolecules* **2004**, *37*, 2861.
[82] J. Chappell, D. G. Lidzey, P. C. Jukes, A. M. Higgins, R. L. Thompson, S. O'Connor, I. Grizzi, R. Fletcher, J. O'Brien, M. Geoghegan, R. A. L. Jones, *Nat. Mater.* **2003**, *2*, 616.
[83] Y. K. Kim, S. A. Choulis, J. Nelson, D. D. C. Bradley, S. Cook, J. R. Durrant, *Appl. Phys. Lett.* **2005**, *86*, 063502.
[84] S. Goffri, C. Müller, N. Stingelin-Stutzmann, D. W. Breiby, C. P. Radano, J. W. Andreasen, R. Thompson, R. A. J. Janssen, M. M. Nielsen, P. Smith, H. Sirringhaus, *Nat. Mater.* **2006**, *5*, 950.
[85] A. C. Arias, J. D. MacKenzie, R. Stevenson, J. J. M. Halls, M. Inbasekaran, E. P. Woo, D. Richards, R. H. Friend, *Macromolecules* **2001**, *34*, 6005.
[86] S. S. van Bavel, E. Sourty, G. de With, J. Loss, *Nano Lett.* **2008**, *9*, 507.
[87] M. G. Harrison, J. Gruner, G. C. W. Spencer, *Phys. Rev. B* **1997**, *55*, 7831.
[88] A. C. Arias, *Polym. Rev.* **2006**, *46*, 103.
[89] F.-C. Chen, Y. K. Lin, C.-J. Ko, *Appl. Phys. Lett.* **2008**, *92*, 023307.
[90] B. Sun, H. J. Snaith, A. S. Dhoot, S. Westenhoff, N. C. Greenham, *J. Appl. Phys.* **2005**, *97*, 014914.
[91] A. Watanabe, A. Kasuya, *Thin Solid Films* **2005**, *483*, 358.
[92] M. P. de Jong, L. J. van Ijzendoom, M. J. Ad. Voigt, *Appl. Phys. Lett.* **2000**, *77*, 2255.
[93] Y. Sahin, S. Alem, R. de Bettingnies, J. M. Nunzi, *Thin Solid Films* **2005**, *476*, 340.
[94] M. M. de Kok, M. Buechel, S. I. E. Vulto, P. van de Weijer, E. A. Meulenkamp, S. H. P. M. de Winter, A. J. G. Mank, H. J. M. Vorstenbosch, C. H. L. Weijtens, Vv. Elsber, in *Physics of Organic Semiconductors* (Ed: W. Brutting), Wiley-VCH, Weinheim, Germany **2005**.
[95] G. Li, C.-W. Chu, V. Shrotriya, J. Huang, Y. Yang, *Appl. Phys. Lett.* **2006**, *88*, 253503.
[96] J. Huang, G. Li, Y. Yang, *Adv. Mater.* **2008**, *20*, 415.
[97] A. Hadipour, B. de Boer, P. W. M. Blom, *Adv. Funct. Mater.* **2008**, *18*, 1.
[98] A. Hadipour, B. de Boer, J. Wildeman, Fs. B. Kooistra, J. C. Hummelen, M. G. R. Turbiez, M. M. Wienk, R. A. J. Janssen, P. W. M. Blom, *Adv. Funct. Mater.* **2006**, *16*, 1897.
[99] G. Dennler, H.-J. Prall, R. Koeppe, M. Egginger, R. Autengruber, N. S. Sariciftci, *Appl. Phys. Lett.* **2006**, *89*, 073502.
[100] J. Gilot, M. M. Wienk, R. A. J. Janssen, *Adv. Funct. Mater.* **2007**, *17*, 143502.
[101] J. Y. Kim, K. Lee, N. E. Coates, D. Moses, T.-Q. Nguyen, M. Dante, A. J. Heeger, *Science* **2007**, *317*, 222.
[102] V. Shrotriya, E. H.-E. Wu, G. Li, Y. Yao, Y. Yang, *Appl. Phys. Lett.* **2006**, *88*, 064104.
[103] H. J. Bolink, E. Coronado, D. Repetto, M. Sessolo, E. M. Barea, J. Bisquert, G. Garcia-Belmonte, J. Prochazka, L. Kavan, *Adv. Funct. Mater.* **2008**, *18*, 145.
[104] D. Gebeyehu, M. Pfeiffer, B. Maennig, J. Drechsel, A. Werner, K. Leo, *Thin Solid Films* **2004**, *451*, 29.
[105] C.-W. Chen, Y.-J. Lu, C.-C. Wu, E. H.-E. Wu, C.-W. Chu, Y. Yang, *Appl. Phys. Lett.* **2005**, *87*, 241121.

[106] C.-W. Chu, C. W. Chen, S. H. Li, E. H. Wu, Y. Yang, *Appl. Phys. Lett.* **2005**, *86*, 253503.
[107] C. J. Brabec, S. E. Shaheen, C. Winder, N. S. Sariciftci, P. Denk, *Appl. Phys. Lett.* **2002**, *80*, 1288.
[108] L. S. Hung, C. W. Tang, M. G. Mason, *Appl. Phys. Lett.* **1997**, *70*, 152.
[109] T. M. Brown, R. H. Friend, I. S. Millard, D. J. Lacey, J. H. Burroughes, F. Cacialli, *Appl. Phys. Lett.* **2001**, *79*, 174.
[110] T. Hasegawa, S. Miura, T. Moriyama, T. Kimura, I. Takaya, Y. Osato, H. Mizutani, *SID Int. Symp. Digest Tech. Papers* **2004**, *35*, 154.
[111] J. Huang, G. Li, E. Wu, Q. Xu, Y. Yang, *Adv. Mater.* **2006**, *18*, 114.
[112] C. J. Brabec, A. Cravino, D. Meissner, N. S. Sariciftci, T. Fromherz, M. T. Rispens, L. Sanchez, J. C. Hummelen, *Adv. Funct. Mater.* **2001**, *11*, 374.
[113] J. Huang, Z. Xu, Y. Yang, *Adv. Funct. Mater.* **2007**, *17*, 1966.
[114] J. Ouyang, Y. Yang, *Adv. Mater.* **2006**, *18*, 2141.
[115] M. S. White, D. C. Olson, S. E. Shaheen, N. Kopidakis, D. S. Ginley, *Appl. Phys. Lett.* **2006**, *89*, 143517.
[116] M. Andersen, J. E. Carle, N. Cruys-Bagger, M. R. Lilliedal, M. A. Hammond, B. Winther-Jensn, F. C. Krebs, *Sol. Energy Mater. Sol. Cells* **2007**, *91*, 539.
[117] S. K. Hau, H.-L. Yip, N. S. Baek, J. Zou, K. O'Malley, A. K.-Y. Jen, *Appl. Phys. Lett.* **2008**, *92*, 253301.
[118] C. Waldauf, M. Morana, P. Denk, P. Schilinsky, K. Coakley, S. A. Choulis, C. J. Brabec, *Appl. Phys. Lett.* **2006**, *89*, 233517.
[119] M. N. M. Glatthaar, B. Zimmermann, P. Lewer, M. Riede, A. Hinsch, J. Luther, *Thin Solid Films* **2005**, *491*, 298.
[120] R. Steim, S. A. Choulis, P. Schilinsky, C. J. Brabec, *Appl. Phys. Lett.* **2008**, *92*, 093303.
[121] T. Ameri, G. Dennler, C. Waldauf, P. Denk, K. Forberich, M. C. Scharber, C. J. Brabec, K. Hingerl, *J. Appl. Phys.* **2008**, *103*, 084506.
[122] L. A. A. Petterson, S. Ghosh, O. Inganäs, *Org. Electron.* **2002**, *3*, 143.
[123] P. A. van Hal, M. P. T. Christiaans, M. M. Wienk, J. M. Kroon, R. A. Janssen, *J. Phys. Chem. B* **1999**, *103*, 4352.
[124] T. J. Savenije, J. M. Warman, A. Goossens, *Chem. Phys. Lett.* **1998**, *287*, 148.
[125] B. C. O'Regan, M. Gratzel, *Nature* **1991**, *353*, 737.
[126] B. A. Gregg, *Chem. Phys. Lett.* **1996**, *258*, 376.
[127] A. C. Arango, L. R. Johnson, V. N. Bliznyuk, Z. Schlesinger, S. A. Carter, H. H. Horhold, *Adv. Mater.* **2000**, *12*, 1689.
[128] P. Ravirajan, D. D. C. Bradley, J. Nelson, S. A. Haque, J. R. Durrant, H. J. P. Smit, J. M. Kroon, *Appl. Phys. Lett.* **2005**, *86*, 143101.
[129] Q. Fan, B. McQuillin, D. D. C. Bradley, S. Whitelegg, A. B. Seddon, *Chem. Phys. Lett.* **2001**, *347*, 325.
[130] C. Y. Kwong, A. B. Djuri, P. C. Chui, K. W. Cheng, W. K. Chan, *Chem. Phys. Lett.* **2004**, *384*, 372.
[131] T.-W. Zeng, Y.-Y. Lin, H.-H. Lo, C.-W. Chen, C.-H. Chen, S.-C. Liou, H.-Y. Huang, W.-F. Su, *Nanotechnology* **2006**, *17*, 5387.
[132] J. Bouclé, P. Ravirajan, J. Nelson, *J. Mater. Chem.* **2007**, *17*, 3141.
[133] K. M. Coakley, M. D. McGehee, *Chem. Mater.* **2004**, *16*, 4533.
[134] G. K. Mor, K. Shankar, M. Paulose, O. K. Varghese, C. A. Grimes, *Appl. Phys. Lett.* **2007**, *91*, 152111.
[135] K. M. Coakley, B. S. Srinivasan, J. M. Ziebarth, C. Goh, Y. Liu, M. D. McGehee, *Adv. Funct. Mater.* **2005**, *15*, 1927.
[136] K. Takanezawa, K. Hirota, Q.-S. Wei, K. Tajima, K. Hashimoto, *J. Phys. Chem. C* **2007**, *111*, 7218.
[137] H.-H. Liao, L.-M. Chen, Z. Xu, G. Li, Y. Yang, *Appl. Phys. Lett.* **2008**, *92*, 173303.
[138] A. H. Sommer, *J. Appl. Phys.* **1979**, *51*, 1254.
[139] J. Xue, B. P. Rand, S. Uchida, S. R. Forrest, *Adv. Mater.* **2005**, *17*, 66.
[140] L. Chen, D. Godovsky, O. Inganäs, J. C. Hummelen, R. A. J. Janssen, M. Svensson, M. R. Andersson, *Adv. Mater.* **2000**, *12*, 1367.
[141] Q. Wei, T. Nishizawa, K. Tajima, K. Hashimoto, *Adv. Mater.* **2008**, *20*, 2211.
[142] D. R. Iyengar, S. M. Perutz, C.-A. Dai, C. K. Ober, E. J. Kramer, *Macromolecules* **1996**, *29*, 1229.
[143] M. Granström, K. Petritsch, A. C. Arias, A. Lux, M. R. Andersson, R. H. Friend, *Nature* **1998**, *395*, 257.
[144] T.-F. Guo, S. Pyo, S.-C. Chang, Y. Yang, *Adv. Funct. Mater.* **2001**, *11*, 339.